China Geology 6 (2023) 494−530

China Geology

Journal homepage: http://chinageology.cgs.cn
https://www.sciencedirect.com/journal/china-geology

Geology and mineralization of the Daheishan supergiant porphyry molybdenum deposit (1.65 Bt), Jilin, China: A review

Nan Ju[a], Di Zhang[a,*], Guo-bin Zhang[b,*], Sen Zhang[c], Chuan-tao Ren[d], Yun-sheng Ren[e, f], Hui Wang[g], Yue Wu[a], Xin Liu[a], Lu Shi[a], Rong-rong Guo[h], Qun Yang[f], Zhen-ming Sun[i], Yu-jie Hao[f]

[a] *Shenyang Center, China Geological Survey, Ministry of Natural Resources (Northeast Geological S&T Innovation Center), Shenyang* 110034, *China*
[b] *Mining College, Liaoning Technical University, Fuxin* 123000, *China*
[c] *Cores and Samples Centre of Natural Resources, China Geological Survey, Ministry of Natural Resources, Langfang* 065200, *China*
[d] *Mudanjiang Natural Resources Survey Center, China Geological Survey, Ministry of Natural Resource, Mudanjiang* 157000, *China*
[e] *Institute of Disaster Prevention, Langfang* 065200, *China*
[f] *College of Earth Sciences, Jilin University, Changchun* 130000, *China*
[g] *School of Earth Science and Resources, Chang'an University, Xi'an* 710000, *China*
[h] *School of Resources and Civil Engineering, Northeastern University, Shenyang* 110031, *China*
[i] *School of Prospecting & Surveying Engineering, Changchun Institute of Technology, Changchun* 130000, *China*

A R T I C L E I N F O

Article history:
Received 3 November 2022
Received in revised form 11 July 2023
Accepted 11 July 2023
Available online 18 July 2023

Keywords:
Molybdenum deposit
Porphyry type
Granodiorite porphyry
Crust-mantle mixing
Metallization
U-Pb age
O-S-Pb isotope
Re isotope
Inclusion type
Ore-bearing fluid
Metallogenic model
Prospecting model
Mineral exploration engineering

A B S T R A C T

The Daheishan supergiant porphyry molybdenum deposit (also referred to as the Daheishan deposit) is the second largest molybdenum deposit in Asia and ranks fifth among the top seven molybdenum deposits globally with total molybdenum reserves of 1.65 billion tons, an average molybdenum ore grade of 0.081%, and molybdenum resources of 1.09 million tons. The main ore body is housed in the granodiorite porphyry plutons and their surrounding inequigranular granodiorite plutons, with high-grade ores largely located in the ore-bearing granodiorite porphyries in the middle-upper part of the porphyry plutons. Specifically, it appears as an ore pipe with a large upper part and a small lower part, measuring about 1700 m in length and width, extending for about 500 m vertically, and covering an area of 2.3 km^2. Mineralogically, the main ore body consists of molybdenite, chalcopyrite, and sphalerite horizontally from its center outward and exhibits molybdenite, azurite, and pyrite vertically from top to bottom. The primary ore minerals include pyrite and molybdenite, and the secondary ore minerals include sphalerite, chalcopyrite, tetrahedrite, and scheelite, with average grades of molybdenum, copper, sulfur, gallium, and rhenium being 0.081%, 0.033%, 1.67%, 0.001%, and 0.0012%, respectively. The ore-forming fluids of the Daheishan deposit originated as the CO_2-H_2O-NaCl multiphase magmatic fluid system, rich in CO_2 and bearing minor amounts of CH_4, N_2, and H_2S, and later mixed with meteoric precipitation. In various mineralization stages, the ore-forming fluids had homogenization temperatures of > 420°C–400°C, 360°C–350°C, 340°C–230°C, 220°C–210°C, and 180°C–160°C and salinities of > 41.05%–9.8% NaCleqv, 38.16%–4.48% NaCleqv, 35.78%–4.49% NaCleqv, 7.43% NaCleqv, and 7.8%–9.5% NaCleqv, respectively. The mineralization of the Daheishan deposit occurred at 186–167 Ma. The granites closely related to the mineralization include granodiorites (granodiorite porphyries) and monzogranites (monzogranite porphyries), which were mineralized after magmatic evolution (189–167 Ma). Moreover, these mineralization-related granites exhibit low initial strontium content and high initial neodymium content, indicating that these granites underwent crust-mantle mixing. The Daheishan deposit formed during the Early-Middle Jurassic, during which basaltic magma underplating induced the lower-crust melting, leading to the formation of magma chambers. After the fractional crystallization of magmas, ore-bearing fluids formed. As the temperature and pressure decreased, the ore-bearing fluids boiled drops while ascending, leading to massive unloading of metal elements. Consequently, brecciated and veinlet-disseminated ore bodies formed.

First author: *E-mail address*: junan-cgs@qq.com (Nan Ju).

* Corresponding author: *E-mail address*: 594139452@qq.com (Di Zhang); zhangguobin000@163.com (Guo-bin Zhang).

Literary editor: Xi-jie Chen
doi:10.31035/cg2023039
2096-5192/© 2023 China Geology Editorial Office.

1. Introduction

Situated in Yongji County, Jilin Province, the Daheishan deposit, a significant molybdenum source, has been in development since the beginning of the 1950s. This deposit, home to 1.09 million tons of molybdenum, is classified as a super-large porphyry molybdenum deposit. Geotectonically, the Daheishan deposit sits at the heart of the Jilin-Heilongjiang orogenic belt (Bi SY et al., 1995), the eastern margin of the Xing'an-Mongolian Orogenic Belt, and is a part of the southern portion of the Xiao Hinggan Mountains–Zhangguangcai Range metallogenic belt. This area underwent the formation and evolution of the Xing'an-Mongolian Orogenic Belt during the Paleozoic (Cai JH et al., 2004). Since the Mesozoic era, it has experienced intense transformations superimposed by the tectono-magmatic activities within the circum-Pacific tectonic domain, leading to widespread metallic mineralization associated with magmatic activity (Chen WM, 1984). In the southern segment of the Xiao Hinggan Mountains–Zhangguangcai Range metallogenic belt (including the Dahei Mountain), large to super-large porphyry molybdenum deposits such as Fu'anpu and Jidetun have been sequentially discovered (Table 1). These deposits, with many similarities in their metallogenic settings and geological characteristics (Lu ZQ, 2017), constitute a characteristic molybdenum deposit concentration area in northeast China. This region bears immense theoretical research significance.

Exploration of the Daheishan deposit, located in Yongji County, began in April 1953, when the No. 204 Geological Team (later renamed as No. 104 Geological Team) of the Northeast Geological Bureau conducted a reconnaissance survey in the area. Upon the advice of Soviet experts, a detailed survey of the mining area was carried out in July, 1954. By 1957, the team completed the exploration, revealing reserves of molybdenum ores with grades above and below the minimum production grade being 964100 t and 126900 t, respectively, as detailed in the report on the Qiancuoluo molybdenum ore reserves (Chang C and Sun JG, 2007). These reserves place the Daheishan deposit among the world's super-large porphyry molybdenum deposits. Moreover, the comprehensive evaluation of associated minerals like sulfur, copper, and gold confirmed that associated useful components such as sulfur and copper all reach the scale of large deposits. The report concluded that the deposit was genetically related to plagiogranites, identifying it as a post-magmatic mesothermal veinlet-disseminated deposit. Further surveys continued in the years that followed. Between 1978 and 1979, the Second Geological Survey Institute of the Geology and Mineral Exploration and Development Bureau of Jilin Province conducted a 1∶50000 regional geological survey in the Wulihe map sheet area. This work led to a preliminary understanding of the alteration and mineralization zones of the Daheishan deposit. The Geophysical Exploration Team of the Geology and Mineral Exploration and Development Bureau of Jilin Province carried out induced polarization (IP) sounding and metallometry in the study area on scales of 1∶50000 and 1∶10000, respectively during the spring of 1980. This identified several IP anomalies. From the autumn of 1980 to the autumn of 1981, the Second Geological Survey

Table 1. Characteristics of major molybdenum deposits in the study area (after Lu ZQ, 2017).

Name	Location	Ore-forming plutons	Mineralization age/Ma	Ore-forming elements	Deposit type	Deposit scale	Data source
Chang'anpu molybdenum (copper) deposit	Shulan City	Monzogranite	168±6.2	Mo (Cu)	Porphyry	Medium	Chen WM, 2002
Chang'anpu molybdenum deposit	Shulan City	Porphyroid monzogranite	171±3	Mo	Porphyry	Medium	Chen YC et al., 1993
Jidetun molybdenum deposit	Shulan City	Granodiorite	169.1±1.8	Mo	Porphyry	Large	Deng PL et al., 1987
Daheishan molybdenum deposit	Yongji County	Granodiorite porphyry	168±4.4	Mo	Porphyry	Supergiant	Han et al., 2014
Xingshan molybdenum deposit	Yongji County	Granodiorite porphyry	167.3±2.5	Mo	Porphyry	Small	Dong SB, 1986
Dashihe molybdenum deposit	Dunhua City	Granodiorite	186.7±5.0	Mo (Fe, Cu, W)	Porphyry	Large	Ju N et al., 2012
Houdaomu molybdenum deposit	Panshi City	Moyite	167.5±1.2	Mo	Porphyry	Medium	Zhang Y et al., 2013
Hongqiling copper-nickel deposit	Panshi City	Olivine pyroxenite	220.6±2	Ni, Cu	Magmatic liquation	Large	Du AD et al., 2001
Piaohe River copper nickel deposit	Jiaohe City	Plagioclase-bearing pyroxenite	217±3	Ni, Cu	Magmatic liquation	Small	Wu FY et al., 2011
Dabinghugou molybdenum deposit	Jiaohe City	Granodiorite	192±3	Mo	Porphyry	Medium	Gao HM, 1995
Erdaodianzi molybdenum deposit	Jiaohe City	Biotite granite	184.1±2.7	Au	Mesothermal	Medium	Wang ZG et al., 2012
Sifangdianzi molybdenum deposit	Huadian City	Fine- to medium-grained granite	176.4±4.2	Mo	Mesothermal	Small	Zhang Y et al., 2013
Lanjiajin deposit	Changchun City	Diorite	170.2±0.3	Au	Skarn	Small	Ge WC et al., 2005

Institute of the Geology and Mineral Exploration and Development Bureau of Jilin Province conducted a reconnaissance survey and prospecting at the periphery of the Daheishan deposit, conducting surface or deep examination and evaluation on the Beishan lead polymetallic ore occurrence and the Yixintun polymetallic ore occurrence in Qiancuoluo, as well as geophysical and geochemical anomalies. From the summer of 1981 to the spring of 1983, the Second Geological Survey Institute conducted a study on the ore factors controlling the nonferrous metals in the Daheishan area. The findings, reported by Wang L (2012), unveiled the deposit 's scale. As of today, the Daheishan deposit holds total proven molybdenum ore reserves of 1.65 billion tons, an average molybdenum ore grade of 0.081%, and molybdenum resources of 1.09 million tons. It has an annual molybdenum concentrate (grade: 47%) production of 8000 t, ranking it as the second-largest molybdenum deposit in both China and Asia and the fifth largest among the top seven molybdenum deposits in the world.

Since 1953, many studies have been conducted on the Daheishan deposit and its surrounding deposits with similar strata, structures, magmatic rocks, minerals, and metallogenic regularities, achieving fruitful results (Wu FY et al., 2000; Zhang YB, 2004; Ge WC et al., 2007; Chen YJ et al., 2007; Wu FY et al. , 2007; Li LX et al., 2009; Wang CH et al., 2009; Ju N et al., 2012; Ju N, 2020; Tang KD et al., 2022). Ge WC et al. (2007) carried out a study on the mineralization age and geodynamic significance of porphyry copper/molybdenum deposits in the eastern segment of the Xing 'an-Mongolian Orogenic Belt. They determined that the granodiorite porphyry related to mineralization and the granodiorites unrelated to mineralization have high-resolution ion micro-probe (SHRIMP) zircon U-Pb ages of 170±3 Ma and 178±3 Ma, respectively. Wang CH et al. (2009) determined the isochron ages of the Re-Os isotopes of molybdenite in the Daheishan deposit at 168.2±3.2 Ma, suggesting that the Daheishan deposit was formed mainly during the Early Yanshanian. Based on the study on the metallogenic stages of the Daheishan deposit and the distribution of ore-bearing fractures in the deposit, Zhou LL et al. (2010) speculated that the Daheishan deposit may have experienced two periods of mineralization and is a typical porphyry deposit. As indicated by thorough research on all the molybdenum deposits in central Jilin, including the Daheishan deposit, the main industrial type of molybdenum ore resources in central Jilin is porphyry-type molybdenum. The ore-forming plutons of all porphyry molybdenum deposits in central Jilin are granitic rocks, and NE- and NW-trending faults are the main rock- and ore-controlling structures. Large-scale molybdenum metallogenic processes, which were closely related to the westward subduction of the Paleo-Pacific Plate, occurred during the late stage of the Early Jurassic or the early stage of the Middle Jurassic (Wang L, 2012; Wang ZG, 2012; Zhang Y, 2013; Hou XG, 2017; Lu ZQ, 2017). These previous studies enrich the basic geological research on the Daheishan deposit and provide a scientific basis for mineral exploration and deposit origin analysis of the deposit. However, few of them focus on the origin of ore-bearing plutons and the spatio-temporal relationship between plutons and mineralization, and it is necessary to deepen the research on the metallogenic model and tectonic setting. On this basis, this study systematically sorts the deposit geology, the intrusion types in the mining area, the petrogeochemistry and isotope geochemistry of ore-bearing plutons, the sources of ore-forming materials, the metallogenic physicochemical conditions, and diagenetic and mineralization ages of the Daheishan deposit. By comparison with other molybdenum deposits of the same type in the study area, this study analyzes the characteristics and origin of the provenance areas of the Daheishan deposit, summarizes the metallogenic regularity and model of the deposit, and builds a prospecting model. This study may serve as a guide for further understanding the metallogenic regularity and origin mechanism of porphyry molybdenum deposits and for conducting prospecting and exploration in deep and edge parts of these deposits.

2. Regional geological setting

The Daheishan deposit, internationally recognized as a representative porphyry molybdenum deposit, is an integral part of the Songnen block, finding its location within the eastern segment of the Xing'an-Mongolian orogenic belt and the southern section of the Xiao Hinggan Range–Zhangguangcai Range metallogenic belt. Geo-tectonically, the deposit marks the eastern extremity of the Central Asian Orogenic Belt and forms part of the southern segment of the Northeast Asian continental margin orogenic belt of the circum-West Pacific region. It is situated in the composite orogenic region of the Paleo-Asian Ocean tectonic domain and the circum-Pacific tectonic domain, positioned between the northeast-trending Yitong–Yilan and Dunhua–Mishan faults. During the Early Yanshanian period, the subduction of the Pacific Plate sparked intense magmatic activity in the study area, which gave rise to considerable mineralization in central and eastern Jilin. This process led to the formation of an array of molybdenum deposits including, but not limited to, Daheishan, Fu 'anpu, Jidetun, Dashihe, Sifangdianzi, and Tianbaoshan. These deposits represent diverse types, such as porphyry, contact metasomatic hydrothermal, and mesothermal quartz vein. As a result of long-term geotectonic evolution, the study area has witnessed several phases of intense tectono-magmatic activity. These periods have fostered the creation of large to super-large endogenetic metallic deposits. Consequently, the area, in conjunction with the Yanbian area in the east, forms the west-east-oriented Jizhong–Yanbian metallogenic belt. This belt, recognized as a significant copper-molybdenum-gold-lead-zinc polymetallic metallogenic belt in northeast China, holds immense potential for further metallogenesis.

Except for the Quaternary, the strata within the study area, all distributed within the Yitong–Shulan fault zone, the Daheishan horst zone, and the Songliao Basin (Fig. 1), present

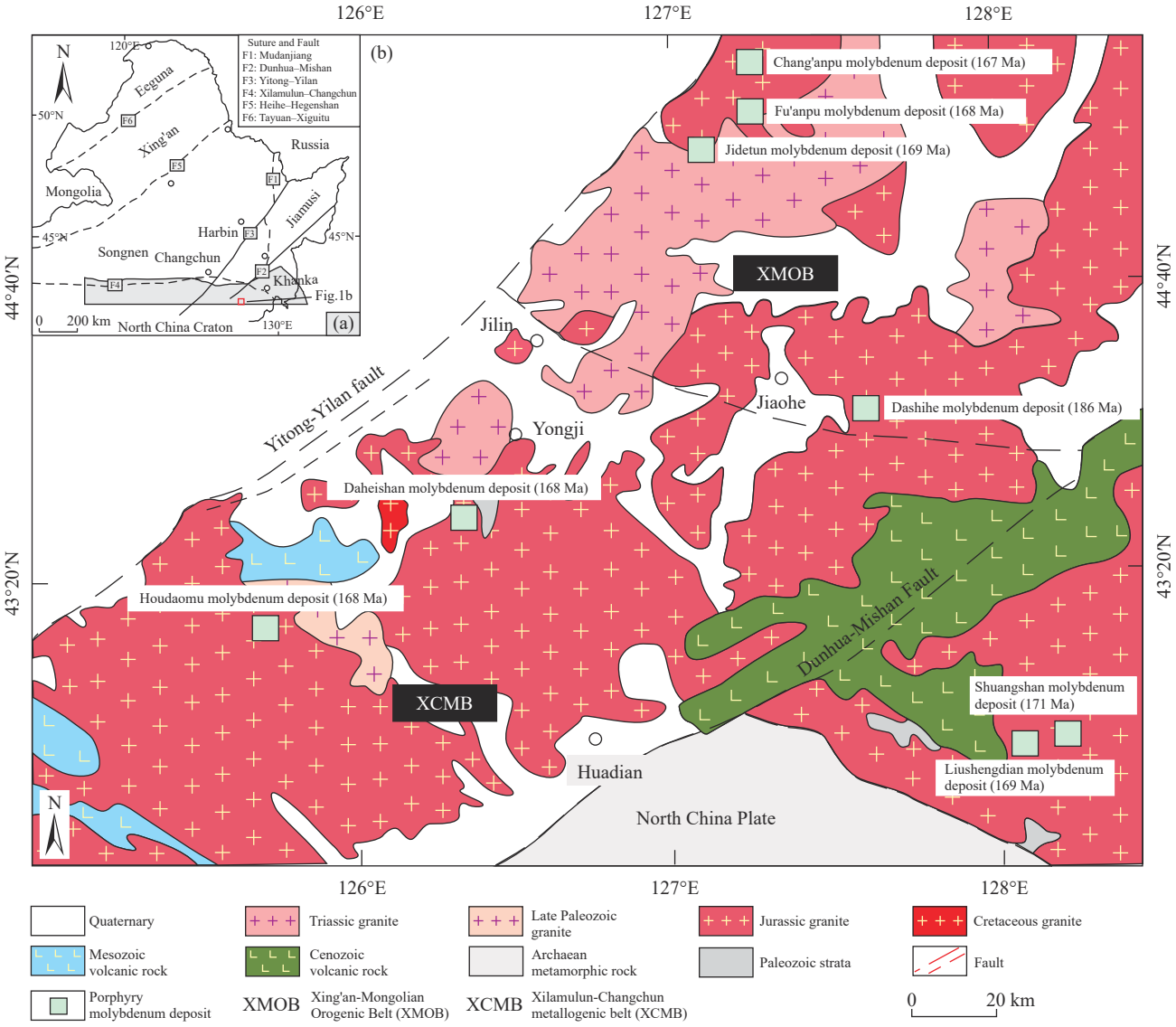

Fig. 1. Geotectonic position and typical molybdenum deposits of the study area (modified from Ju N, 2020).

a diverse geological chronology ranging in age from the Proterozoic to Quaternary periods. Starting with the oldest, these strata include the Proterozoic Xinxing, Jifanggou, and Galashan formations (Table 2). Following these are the Paleozoic Toudaogou, Huangyingtun, Xiaojingou, Laotudingzi, Luquantun, Mopanshan, Zhesi, Wudaogou (Group), Fanjiatun, Daheshen, and Wudaoling formations. Mesozoic strata include the Sihetun, Nanloushan, Erlanghe, Yuxingtun, Chang 'an, Ningyuancun, and Yingcheng formations, which are then succeeded by the Cenozoic Jishu, Chuandishan, and Junjian formations. The most recent strata include those from the Quaternary period, specifically the Pleistocene and Holocene, as well as terraces and floodplain deposits found on either side of the main river valleys within the study area (Hu SX, 1988; Ge XH, 1990; Han YW et al., 2003; Hou ZQ et al., 2003; Ji KJ et al., 2011).

The study area has experienced considerable tectonic evolution from the Paleozoic era through the Middle Triassic period. Initially, it was shaped by the subduction of the Paleo-Asian Ocean, giving rise to regional NE- and NW-oriented structures (Jiang PM, 1989). Subsequently, from the Late Triassic onward, the area underwent the evolution of the Paleo-Pacific tectonic domain, resulting in a tectonic framework chiefly defined by NE-NNE- and NW-NNW-oriented tectonic lines, complemented by EW- and SN-oriented lines.

Intrusive rocks are abundant in the study area, making up over two-thirds of the bedrock outcrop area, existing as batholiths or stocks. These rocks document a magmatic progression from mafic to intermediate, and eventually, to intermediate-acid compositions (Table 3). The Jizhong area has experienced frequent and intense tectono-magmatic activities since the Paleozoic era due to the superposition and transformation of the Paleo-Asian Ocean tectonic domain and the Paleo-Pacific tectonic domain (Li JH et al., 1978; Li CY et al., 1983; Li JA et al., 1984; Li N, 1993). The study area is characterized by widely distributed Mesozoic intrusive rocks, alongside some Late Paleozoic intrusive rocks and a few of Early Paleozoic intrusive rocks. Predominantly granitic, these Paleozoic–Mesozoic intrusive rocks are sporadically

Table 2. Meso-Cenozoic stratigraphic correlation of the study area (after Zhang Y, 2013).

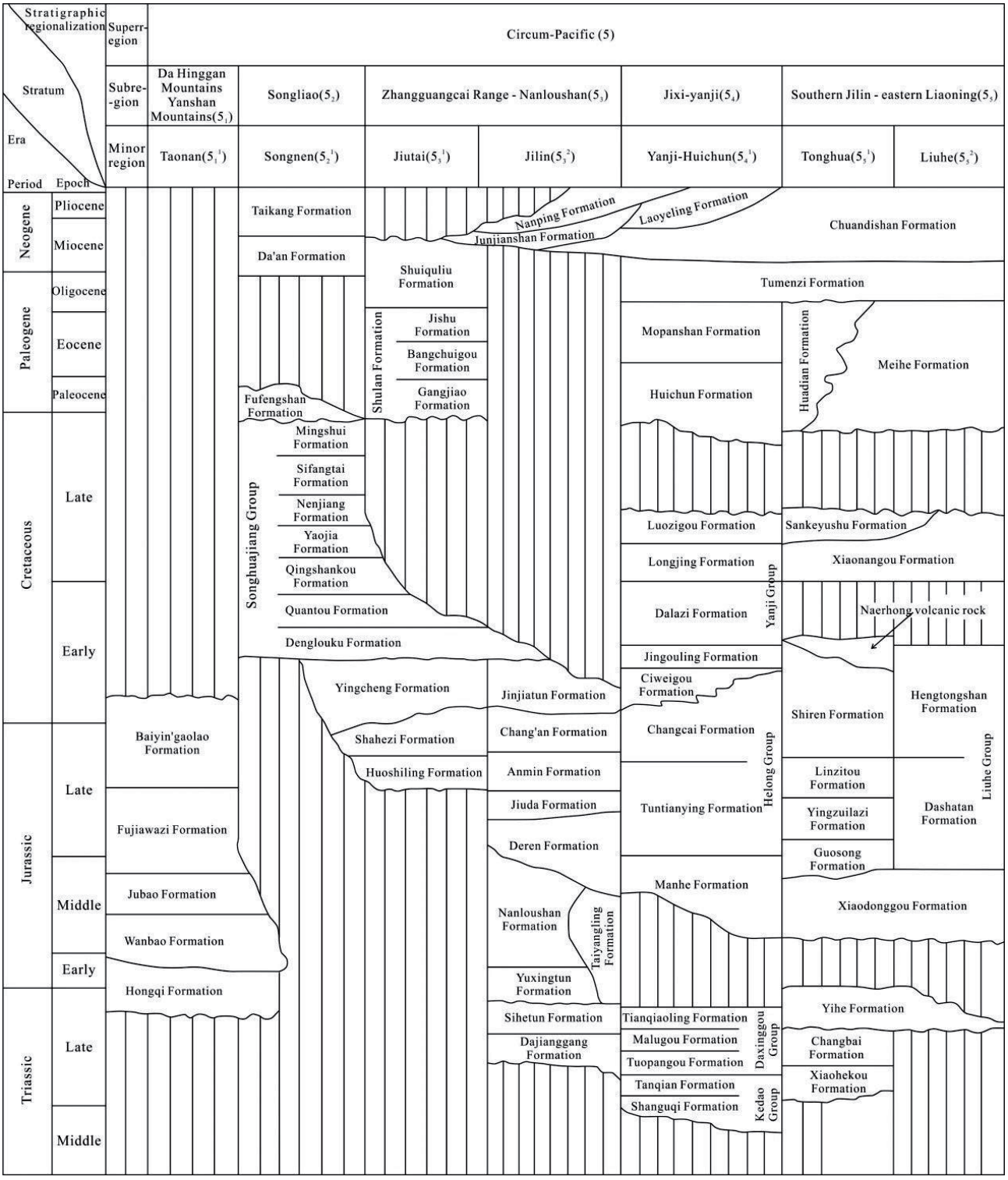

interrupted by mafic-ultramafic intrusive rocks.

Given its unique geotectonic location, the study area has witnessed and endured substantial geological processes such as the convergence of minor blocks in the Paleo-Asian Ocean tectonic domain, the accretion of terranes within the circum-Pacific tectonic domain, and the superimposition and transformation of these two primary tectonic domains (Lu HZ, 1990, 1995; Liu B et al., 1999). The multiphase and intricate tectono-magmatic activity has positioned the study area as a significant molybdenum ore resource region within China, drawing considerable attention and research.

3. Geological characteristics of the mining area

3.1. Strata

The eastern and southeastern portions of the mining area encompass the Lower Paleozoic Toudaogou Formation, acting

Table 3. Statistics of Mesozoic igneous rocks in the study area (after Zhang Y, 2013).

Era	Pluton	Lithology	Age/Ma	Dating method	Source
Triassic	Qinglinzi	Hornblende syenite	223±1	SHRIMP	Zhang YB, 2004
	Hongqiling	Olivine pyroxenite	220.6±2	LA-ICP-MS	Liu B, 1987
	Sandaohe	Syenogranite	216±3		Lu HZ et al., 2004
	Naozhigou	Monzogranite	214±10	SHRIMP	Zhang YB, 2004
	Qishi'ergedingzi	Monzogranite	206±4		
	Dahuanggou	Granodiorite	203±2		
Jurassic	Tianqiaogang	Alkali-feldspar granite	188±4	TIMS	Lu JM et al., 2007
	Daxinggou	Granodiorite	187±1	SHRIMP	Zhang YB, 2004
	Xinhualong	Granodiorite porphyry	183.8±1.1	LA-ICP-MS	Zhang Y, 2013
	Tianqiaogang	Alkali-feldspar granite	182±3	SHRIMP	Lu JM et al., 2007
	Jidetun	Granodiorite	170.9±0.8	LA-ICP-MS	Zhang Y, 2013
	Daheishan	Granodiorite porphyry	170±3	SHRIMP	Ge WC et al., 2007
	Huangniling	Monzogranite	168±3		Zhang YB, 2004
	Fu'anpu	Monzogranite	167±0.8	LA-ICP-MS	Zhang Y, 2013
	Chang'anbu	Granodiorite porphyry	166.9±1.5		
	Dongqing	Alkali-feldspar granite	162±1	SHRIMP	Zhang YB, 2004
Cretaceous	Zhongping	Diorite	129±2		
	Xiaoxi'nancha	Granitic complex	115–106		Qu XM et al., 2004

as the immediate surrounding rocks for the Daheishan deposit 's ore-forming plutons. The upper part of this formation consists of metasandstones, phyllitic slates, and plagioclase actinolites interspersed with marble lenses. The middle part also consists of plagioclase actinolites interbedded with marble lenses, while the lower part comprises plagioclase actinolites mingled with metasandstones, metamorphic intermediate to intermediate-acid tuffs, volcanic breccias, rhyolites, dacites, and andesites (Fig. 2). The near-ore lithology of the Toudaogou Formation features gray to grayish-green plagioclase actinolites, biotite hornfels, grayish-white diopside hornfels, and black slates interbedded with sucrosic marble lenses. Previous measurements of trace elements in the Toudaogou Formation show molybdenum content exceeding the average value of corresponding rocks in the crust, with molybdenum concentrations of 30×10^{-6} and 65×10^{-6}–75×10^{-6} in lavas and tuffaceous rocks, respectively. The Mesozoic Upper Triassic Nanloushan Formation is exposed in the eastern and southern sections of the mining area, predominantly composed of gray rhyolitic breccia-bearing crystal tuffs, rhyolitic crystal tuffs, and dacitic crystal tuffs intermingled with thinly laminated black tuffaceous slates.

3.2. Structures

The ore-forming plutons of the Daheishan deposit are situated in the EW-trending uplift-fault belt and at the core of the Qiancuoluo overturned anticline comprised of Lower Paleozoic strata. It 's also located at the margin of the Mesozoic volcanic faulted basin and the intersection of the EW-trending basement fault zone and NE-trending faults. The structures within the study area can be classified into three groups: (1) EW-directed structures, predominantly composed of compressive faults; (2) an overturned syncline, with crumpled structures and bedding faults developing inside; (3) NE-trending compressive faults and NW-trending torsional faults. The ore-forming porphyry plutons are found in the composite area of these structures.

3.2.1. Fold structures

The regional basement structure within the study area is composed of Caledonian and Late Hercynian to Early Indosinian structural layers, which collectively form the main body of the Jizhong synclinorium. The Hercynian tectonic activity gave rise to compact, linear, and overturned folds. These folds are generally arcuate along the axis, with the arch apex extending westward. Associated with these folds are strike-thrust faults, as well as NE- and NW-trending torsional faults, exhibiting a dense zonation pattern.

3.2.2. Fault structures

The predominant fault structures are the result of Mesozoic tectonic activity (Fig. 3). In addition to the NE-directed volcanic-magmatic tectonic belt, numerous NNE-trending faults, such as the Kouqian-Liuhe fault zone, and associated NW-trending faults were formed. During this period, relatively older faults, like the NE-trending Yitong-Shulan and Dunhua-Mishan faults, experienced inherited torsion. Concurrently, the EW-trending faults, including the Daheishan-Cuoluotun-Tudaogou paleo-uplift zone, experienced renewed uplift. This formed an uplift-fault belt that spanned approximately 20 km from north to south and about 50 km from east to west. This uplift-fault belt played a critical role in shaping the molybdenum ore field. Tectonic movements triggered magmatic intrusion. Where NE- and EW-trending basement faults intersected with NW-trending faults, the eruption of intermediate-acidic magmas ensued, followed by the intrusion of mafic-intermediate-acidic magmas. This led to the formation of the Jizhong volcanic-intrusive complex. As a result, a joint rock- and ore-controlling tectonic framework was established. The joint fissures corresponding to large-scale NE- and EW-trending faults provide favorable conditions for molybdenum ore enrichment.

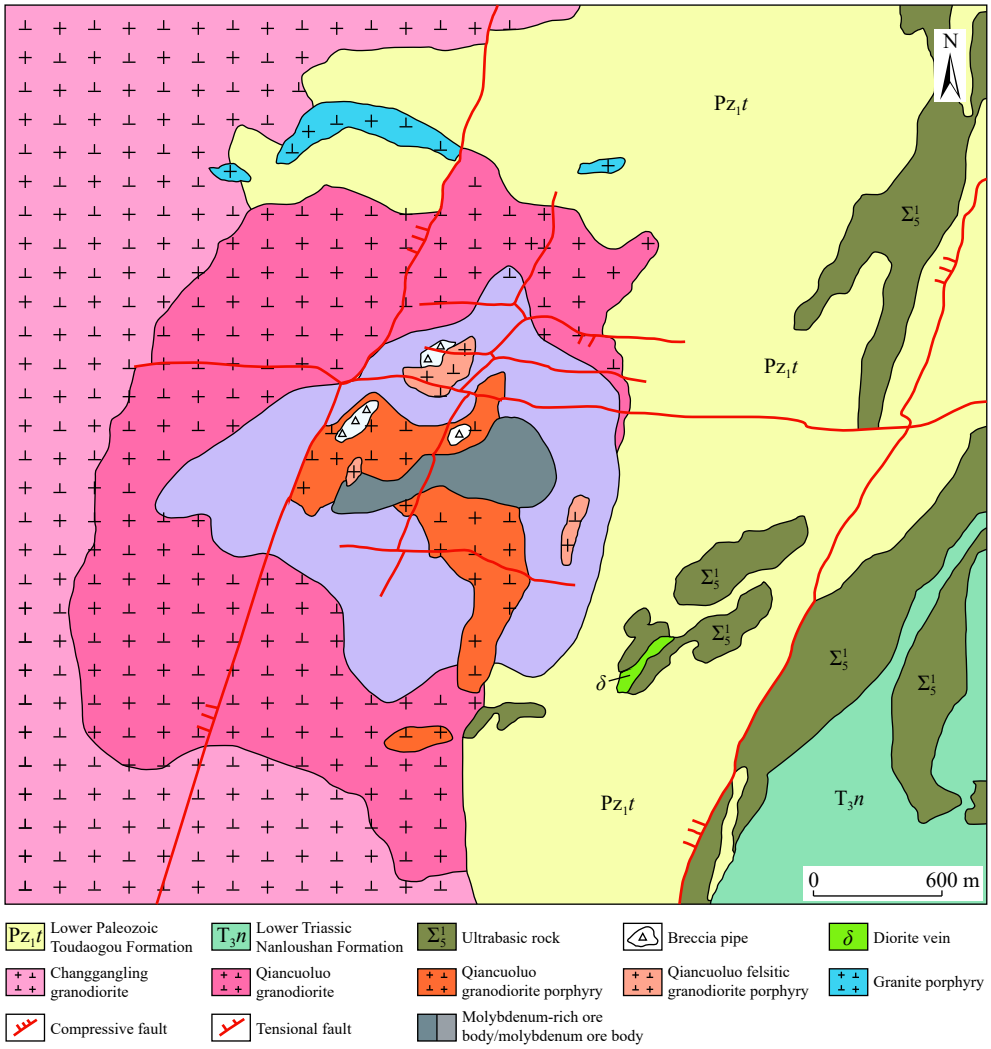

Fig. 2. Geological map of the Daheishan mining area (after Hou XG, 2017).

3.2.3. Ore-controlling breccia pipes

Breccia pipes are significantly developed in the Daheishan deposit. The creation of ore-bearing breccias may be attributed to the expansion caused by the escape of volatile constituents from magmas during the ascent and emplacement of granodiorite porphyries. As magma crystallization progressed and anhydrous minerals formed, magmas became increasingly volatile, which increased the vapor pressure. With falling temperatures and escalating vapor pressure, the magmas degraded and boiled, resulting in the significant escape of gas and violent expansion. Brecciation occurred swiftly and extensively when the vapor pressure brought about by expansion surpassed the tensile strength of the external intrusive rocks. This study posits that the breccia pipes and fractures, which were formed due to hydraulic fracturing in the brecciation process, are the primary ore-bearing structures. This contrasts with the previous conclusion that molybdenum mineralization is unassociated with these structures.

3.3. Intrusive rocks

The primary intrusive rocks within the mining area encompass medium- to fine-grained granites, K-feldspar granite porphyries, granodiorites, inequigranular granodiorite porphyries, molybdenum-bearing granodiorite porphyries, diorites, and quartz diorites. These rocks occur as batholiths or stocks. Mafic-ultramafic rocks, porphyrites, and granite porphyries also exist, taking the form of walls or veins. The ore-bearing plutons are complex plutons, taking an elliptical form in the planar view and extending 8 km in length and 3.5 km in width in the northeast direction. Recent research from the Second Geological Survey Institute of the Geology and Mineral Exploration and Development Bureau of Jilin Province identifies four phases of intrusive rocks, as presented in Table 4. Regarding regional rock-controlling characteristics, the emplacement of the ore-bearing complex plutons was regulated by EW-trending faults. In contrast, the morphologies of the plutons were controlled by intersections of NE- and EW-trending faults, in addition to overturned anticlines and their turning parts. The formation of the ore-bearing complex plutons of the Daheishan deposit coincided with several cryptoexplosions, leading to the local formation of cryptoexplosive breccias.

The Changgangling biotite granodiorite pluton of the first phase is in intrusive contact with the Lower Paleozoic Doudaogou Formation and the Late Triassic Nanloushan

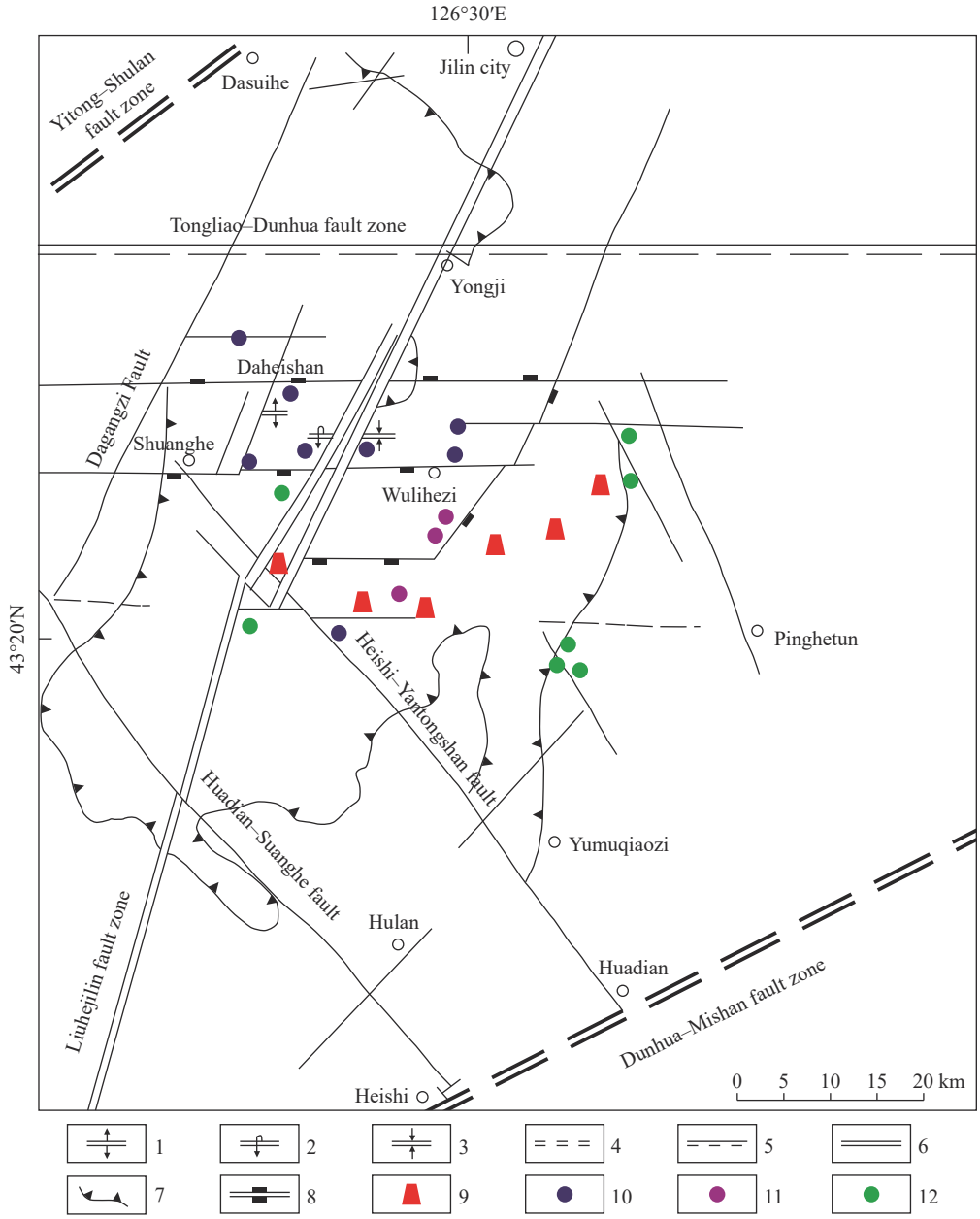

Fig. 3. Structural outline map of the Daheishan mining area (after Lu ZQ, 2017). 1–Anticlinal axis; 2–overturned anticlinal axis; 3–synclinal axis; 4–deep fault zone; 5–fault zone inferred; 6–crustal fault; 7–Mesozoic volcanic faulted area; 8–E-W-trending upfaulted zone; 9–crater; 10–molybdenum deposit (ore occurrence); 11–copper deposit (ore occurrence); 12–polymetallic deposit (ore occurrence)

Formation. As revealed by trenching in the Beishan Mountain of the Daomuhetun area, this granodiorite pluton intruded into the dacitic volcanic rocks of the Nanloushan Formation. This pluton on the side of the contact zone shows significantly small mineral particles, forming a cooling edge with a width of about 1 m. Many xenoliths of surrounding rocks occur in the pluton, with sizes varying in the range of 1–40 cm. The volcanic rocks in the surrounding rocks show significant mineral recrystallization and a baking edge with a width of about 5–10 cm, which is brown due to weathering. The Beishan granodiorite pluton in the Houcuoluotun area was invaded by the Early Jurassic Dadingzi granite pluton, which forms a cooling edge with a width of 10 cm near the contact zone.

As for the Qiancuoluo inequigranular biotite granodiorite pluton of the second phase, its north and east sides are in intrusive contact with the Toudaogou Formation, and its south and west sides intruded into the marginal fine-grained granodiorites of the Changgangling granodiorite pluton. The clear contact boundary between the two plutons and the absence of cooling and baking edges indicate a short time interval between the formation of both plutons. The xenoliths of surrounding rocks are widely distributed in the biotite granodiorite pluton, especially in its eastern half. The xenoliths are dominated by the metamorphic intermediate-mafic volcanic rocks of the Toudaogou Formation, followed by metasandstones and minor quantities of marbles and ultramafic rocks. At the western boundary of the pluton is the residual cover of the marginal fine-grained biotite granodiorites of the Changgangling pluton.

Table 4. Statistics of intrusive rocks in the Daheishan mining area (after Lu ZQ, 2017).

Pluton	Changgangling biotite granodiorite	Qiancuoluo inequigranular granodiorite	Qiancuoluo inequigranular granodiorite porphyry	Qiancuoluo felsitic granodiorite porphyry
Morphology	Elliptical	Elliptical	Irregular	Crescent
Scale	Length: 8 km, width: 3.5 km, area: 28 km^2	Length: 2.25 km, width: 1.65 km, area: 3.7 km^2	Length: 0.9 km, width: 0.35 km, area: 0.46 km^2	Length: 0.275 km, width: 0.14 km, area: 0.038 km^2
Attitude	NE-trending long axis, pitch direction: southeast	NE-trending long axis, dip direction: NW, dip direction: 80°	W-E-trending long axis, dip direction: south, 70°–80°	W-E-trending long axis, dip direction: south, 70°–80°
Textures and structures	Hypidiomorphic granular textures, with porphyroid or porphyritic textures locally; lumpy structures	Hypidiomorphic granular textures and inequigranular porphyroid textures; lumpy structures	Porphyritic textures primarily, with porphyroid or porphyroclastic textures partially; matrix showing hypidiomorphic granular textures and microscopic anhedral granular textures or felsic textures; lumpy and brecciated-mottled structures	Dominated by porphyritic textures, with porphyroclastic textures locally; matrix showing felsic textures; lumpy structures
Mineral assemblages	Lithogenetic minerals: quartz, plagioclase, alkali feldspar, and biotite; accessory minerals: sphene, zircon, apatite, rutile, magnetite, etc.	Lithogenetic minerals: plagioclase, quartz, alkali feldspar, and a small amount of biotite; accessory minerals: zircon, apatite, rutile, magnetite, etc.	The speckles: plagioclase and quartz primarily, with a small amount of alkali feldspar and biotite; accessory minerals: zircon, sphene, apatite, magnetite, etc.	Phenocryst minerals: plagioclase, quartz, alkali feldspar, and a small amount of biotite; accessory minerals: zircon, apatite, rutile, pyrite, etc.
Isotopic age/Ma	1784±0.9	169.9±2.3	169.9±0.9	
Contact relationship	Intrusive contact with the Lower Paleozoic Toudaogou Formation and the Late Triassic Nanloushan Formation	Intrusion into the Toudaogou Formation in the north and east and the Changgangling granodiorite plutons in the south and west	Intrusion into inequigranular biotite granodiorites	Intrusion into inequigranular biotite granodiorites and granodiorite porphyries

The Qiancuoluo granodiorite porphyries of the third phase intruded into inequigranular granodiorites. Quartz veins are found to be filled along the contact zone between their contact zone at the surface and depth. The upper part of the porphyries hosts various breccias as surrounding rocks. Besides a few strata and ultramafic breccias, these breccias are dominated by inequigranular granodiorite breccias.

The Qiancuoluo felsitic granodiorite porphyries, in the form of apophyses or veins, intruded into inequigranular granodiorites the granodiorite porphyries. These apophyses and veins exhibit significantly different alteration characteristics from their surrounding rocks. Specifically, they lack the quartz-sericite alteration widespread in surrounding rocks and host weak molybdenum mineralization. These phenomena suggest that the intrusion of the felsitic granodiorite porphyries occurred after the dominant mineralization period.

Overall, the Daheishan complex plutons in the area are distributed in the Changgangling–Qiancuoluo area, extending in the NNE direction. They take an elliptical shape planarly, with a length of 8 km, a width of 4 km, and an area of about 32 km^2. Their morphologies and distributions vary with geological structures.

4. Alteration and mineralization

4.1. Ore body

The main ore body of the Daheishan deposit is a large, single ore body simply shaped ore pipe with a large upper part and a small lower part, measuring approximately 1700 m in length and width, covering an area of 2.3 km^2, and extending vertically for around 500 m (Fig. 4). It appears irregularly round in a planar view, with its top eroded away. The high-grade ores of the deposit are partially centered and partially suspended in the middle-upper part of the ore body, which has a NE strike and extends in only one direction. However, due to its large cross-section and approximately round appearance on the ground surface, the main ore body of the Daheishan deposit appears as a large-scale ore pipe. Exploration data were used to delineate three annular contours within ore-bearing plutons, corresponding to molybdenum grades of 0.08%, 0.04%, and 0.02% sequentially outwards. The inner annular contour displays a dumbbell shape with a west-east length of about 160 m and a north-south width of 140–320 m. The middle annular contour shows a pear shape with a west-east length of about 800 m and a north-south width of about 700 m, while the outer annular contour displays a round shape with a diameter of about 1000 m. Furthermore, the main ore body of the Daheishan deposit appears columnar in the profile. Accordingly, it resembles a pot that gradually tapers downward.

The main ore body occurs primarily within granodiorite porphyry plutons and their surrounding inequigranular granodiorite plutons, with the majority of the high-grade ores located in the ore-bearing granodiorite porphyries in the middle-upper part of the porphyry plutons (Fig. 5). However, the high-grade ores do not spatially or originally correlate with cryptoexplosive breccia pipes. The southeastern portion of the main ore body extends narrowly into the metamorphic intermediate-mafic volcanic rocks of the Lower Paleozoic Toudaogou Formation. The intensity of mineralization gradually diminishes from the center of the ore body to its

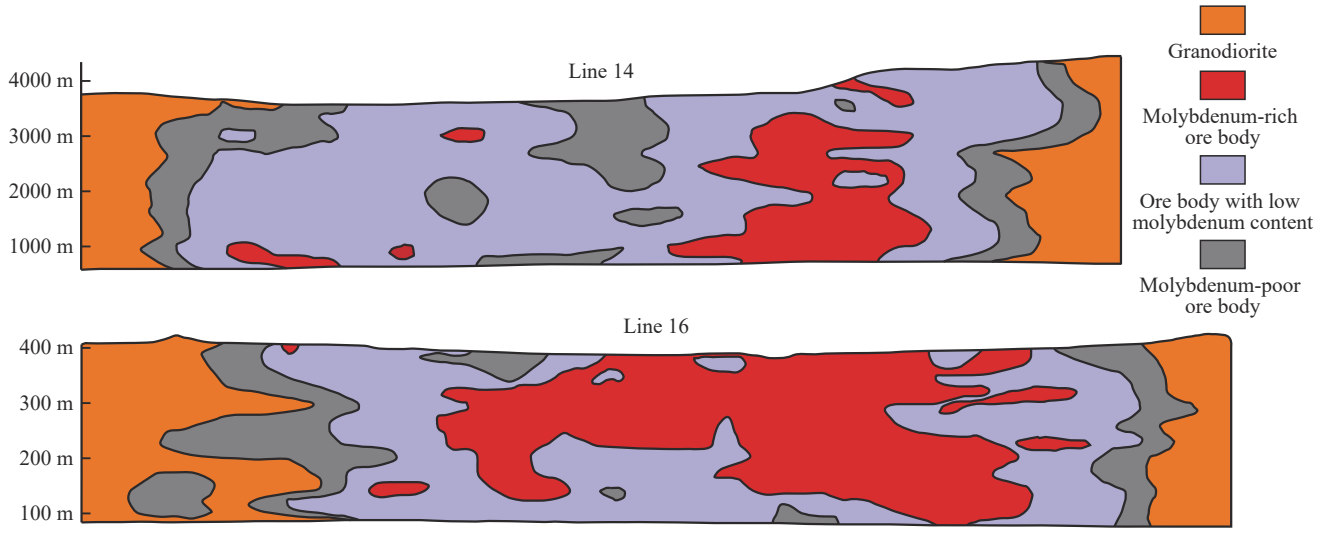

Fig. 4. Profiles of ore bodies along lines 14 and 16 in the Daheishan molybdenum deposit (after Hou XG, 2017).

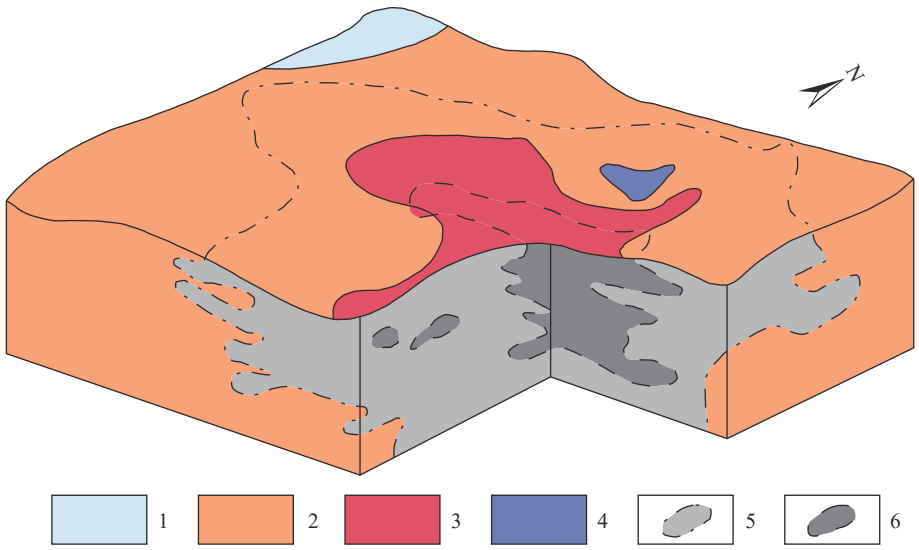

Fig. 5. 3D profile of the main ore body of the Daheishan molybdenum deposit (after Lu ZQ, 2017). 1–Changgangling granodiorite; 2–Qiancuoluo inequigranular granodiorite; 3–Qiancuoluo granodiorite porphyry; 4–felsitic granodiorite porphyry; 5–low-grade ore body (Mo grade: 0.02% –0.08%); 6–high-grade ore body (Mo grade: > 0.08%)

periphery, and no distinct boundaries exist between the ore body and its surrounding rocks or between low-grade and high-grade ores. The mineralization shows concentric zonation, exhibiting molybdenite, chalcopyrite, and sphalerite horizontally from the center outward and molybdenite, azurite, and pyrite vertically from top to bottom. The main ore body shows elemental zones of Mo, Cu, Pb, and Zn from the center outward. In a planar view, molybdenum grade is high in the center and decreases outward. In the vertical direction, the sulfur grade increases at depths greater than 200 m, and the gold grade correlates positively with the pyrite grade. The main ore body's top, especially the top of high-grade ores, frequently hosts inequigranular granodiorites and minor amounts of breccias or xenoliths of surrounding rocks of the Toudaogou Formation. This suggests that mineralization and enrichment have extended beyond the top of the porphyry plutons and into surrounding rocks. Beneficial associated elements like copper, lead, zinc, and silver are relatively enriched at the edges of the main ore body. The quartz-K-feldspar alteration, widely exposed on the ground surface, is distributed concentrically from the center of the ore body outward together with quartz-sericite and propylite alteration zones. These findings suggest that the Daheishan deposit may have undergone moderate denudation.

The upper part of the Daheishan deposit contains oxidation zones and mixed mineralized belts, with the oxidation transition zones typically found at a depth of 10–35 m. The North China climate makes it difficult for secondary enrichment zones to form. Copper mineralization associated with granodiorites in the Duobaoshan ore block primarily occurs in the inner and outer contact zones between the plutons and the surrounding rocks. The main ore body is largely located in the outer contact zones, extending downwards into the plutons. Thicker and larger ore blocks

mostly occur near the top strata, that is, near the edges of the inner contact zones. Existing knowledge of the ore body reveals that when the outer contact zones have a mineralization range with a width of 200 m and a thickness of 50 m, the copper ore bodies in the lower inner contact zones will expand correspondingly, forming thicker and larger ore bodies. The porphyry copper mineralization associated with granodiorite porphyry intrusions mainly formed in the outer contact zones of the porphyry plutons, with the main ore body distributed primarily in the upper part of the periphery of the granodiorite porphyry plutons. The mineralization is more prominent in the hanging wall (southwest) of the porphyry plutons than in its foot wall and is at a higher degree in the pitching part (northwest) than in the tilted part.

In terms of spatial distribution, the ore bodies are all distributed in a circular pattern around porphyry plutons. The major ore body is largely distributed in the upper part around the major porphyry plutons, generally 0–500 m away from the latter. The most intense mineralization is observed at a distance of 50–150 m away from the porphyry plutons, where the ore grades are high and the mineralization is uniform. The mineralization gradually weakens towards either side. The porphyry plutons at burial depths exceeding 500 m frequently correspond to ore bodies with large burial depths as well. In instances where the porphyry pluton has undergone substantial denudation, only a few ore body branches with small extensions remain on the hanging wall and foot wall of the porphyry plutons. Some dykes tend to occur in the upper part of the porphyry plutons, and the mineralization alteration and mineralization around are generally weak (Ma HW, 1990; Luo MJ et al., 1991; Pei RF, 1995; Rui ZY et al., 2004).

4.2. Ore minerals

The molybdenite in the Daheishan deposit is filled in the fractures or joints of rocks in the form of veinlets or occurs on both sides of quartz veinlets. Some of it is disseminated, distributed uniformly in granodiorites. Besides, some molybdenite scatters in slightly altered sections and at the edges of ore bodies in the form of star-shaped coarse crystals.

4.2.1. Composition of ore minerals

In the Daheishan deposit, major ore minerals include pyrite and molybdenite, while minor minerals include sphalerite, chalcopyrite, tetrahedrite, and scheelite The major characteristics of these ore minerals are as follows (Fig. 6).

Molybdenite: molybdenite in the Daheishan deposit is lead gray, with a metallic luster and gray-black streaks. It mostly occurs as semi-idiomorphic or anhedral crystals, while a small amount of coarse-grained molybdenite appears as idiomorphic crystals. It reflects a grayish-white color and exhibits significantly varying reflection pleochroism. Its crystals are frequently in the shape of curved flakes or leaves, displaying wavy extinction and even a phenomenon similar to kinks in deformed rocks. Cleavages are very common in the molybdenite. Additionally, the molybdenite exhibits bireflection, non-significant internal reflection colors, and

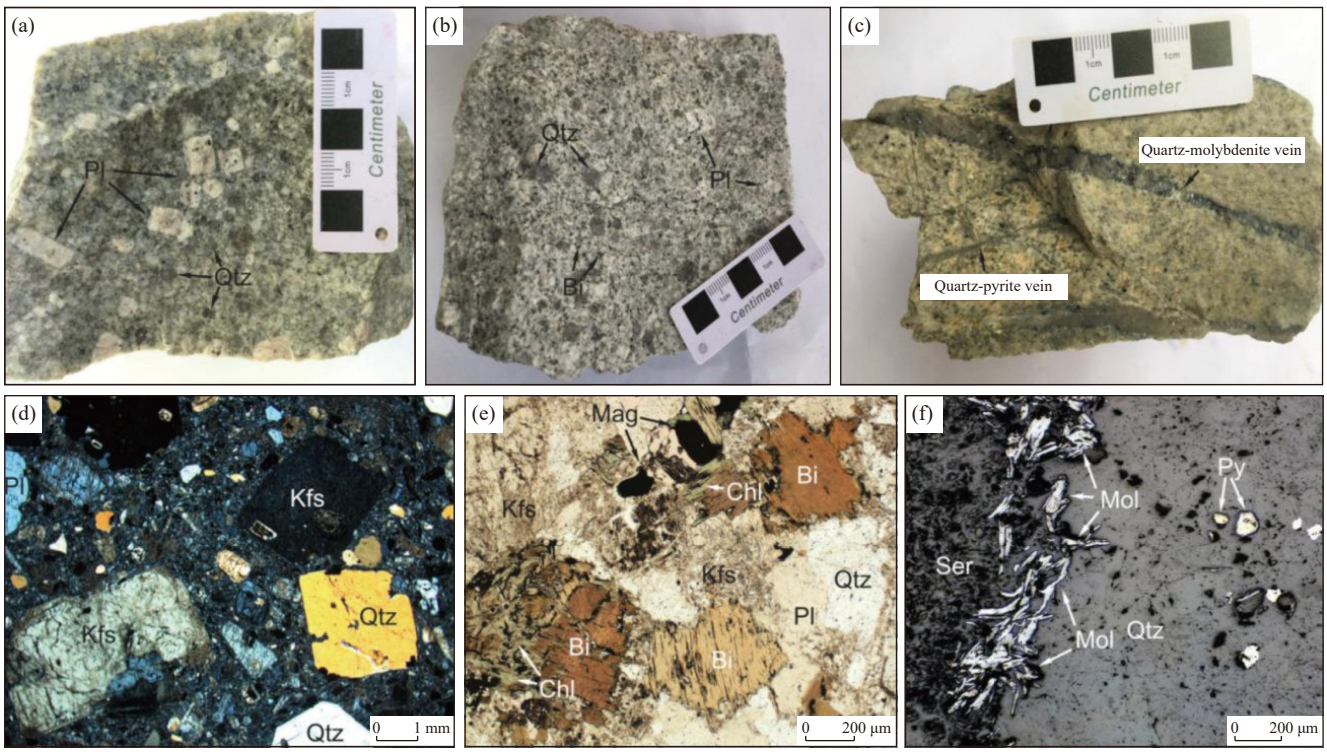

Fig. 6. Hand specimens and photomicrographs of ores from the Daheishan molybdenum deposit (after Xing K, 2021). (a)–Granite porphyry; (b)–biotite monzogranite; (c)–granite porphyry bearing quartz molybdenite veins and quartz pyrite veins; (d)–granite porphyry; (e)–biotite monzogranite, with magmatic biotite becoming epidote due to hydrothermal alteration; (f)–quartz molybdenite veins with sericite-quartz alteration under reflected light. Note: Bi–biotite; Chl–epidote; Kfs–feldspar; Mol–molybdenite; Pl–plagioclase; Py–pyrite; Qtz–quartz; Ser–sericite-quartz alteration

high heterogeneity.

Pyrite: pyrite in the Daheishan deposit is yellow to light brassy yellow, with a metallic luster, high hardness, and greenish-black streaks. Iridescence is common on its surface. The pyrite occurs as hypidiomorphic crystals mostly and idiomorphic crystals partially. It reflects a light-yellow color (yellowish-white), without pleochroism. Regarding morphologies, it occurs as homogeneous cubic, pentagonal dodecahedral, and octahedral idiomorphic crystals. It has greatly varying grain sizes of 0.02–2 mm dominated by 0.5–1 mm. It frequently presents dissolution textures after being metasomatized by chalcopyrite, sphalerite, quartz, and calcite or cataclastic textures under the action of force. In addition, the pyrite shows an eroded surface and local cataclastic textures due to its fragility.

Sphalerite: sphalerite in the Daheishan deposit is yellow or light yellow, with a light-green or light-blue tone and vitreous-adamantine lusters. It is translucent, brittle, and anhedral granular. It presents distinct triangular striations, with grain sizes of mostly about 0.1 mm. It, together with chalcopyrite, frequently forms exsolution textures. Some of it contains chalcopyrite in the form of droplet-shaped inclusions, with veinlet-like sphalerite observed to penetrate pyrite. The sphalerite is homogeneous and shows a yellow internal reflection color, without pleochroism and bireflection.

Chalcopyrite: chalcopyrite in the Daheishan deposit is brassy yellow and hypidiomorphic or anhedral granular, with a strong metallic luster and blackish-green streaks. It shows conchoidal fractures, without cleavages. Blue-violet iridescence is frequently visible on its grain surfaces. It has low hardness and grain sizes of 0.07–0.2 mm dominated by about 0.1 mm. It reflects a brassy yellow and is weak heterogeneity, without idiomorphic crystals, pleochroism, or internal reflection color.

Tetrahedrite: tetrahedrite in the Daheishan deposit is closely associated with chalcopyrite, showing similar metallogenic stages and spatial distribution except that the former has a lower tetrahedrite content. The tetrahedrite is iron-black, with an asphalt-like or submetallic luster, pink to brown streaks, and low hardness. It has a smooth surface, flat fractures, anhedral granular textures, and grain sizes of 0.07–0.2 mm dominated by about 0.1 mm. It is usually associated with chalcopyrite, rarely occurring alone. In addition, it primarily occurs in quartz veins bearing molybdenite and pyrite.

Scheelite: scheelite in the Daheishan deposit is white or light yellow and translucent, with a strong silky luster and colorless streaks. It is extremely brittle and hypidiomorphic or anhedral granular, with grain sizes of 0.07–0.15 mm dominated by around 0.1 mm. It primarily formed during the high-temperature gas-liquid quartz-K-feldspar alteration, occurring in quartz-K-feldspar veins and quartz veinlets.

Besides, the Daheishan deposit contains traces of gold, bismuthinite, pyrrhotite, magnetite, ilmenite, arsenopyrite, lillianite, marcasite, and clausthalite. Its secondary minerals include limonite, malachite, cerusite, wulfenite, and molybdite. It also has non-metallic minerals such as quartz, feldspar, biotite, actinolite, and diopside, as well as altered minerals such as sericite and chlorite. Regarding the metal sulfide assemblages, their contents are in the order of pyrite > molybdenite > sphalerite > chalcopyrite > tetrahedrite, consistent with the metal sulfide assemblages and the content ranking of some typical porphyry copper (molybdenum) deposits at home and abroad.

4.2.2. Ore textures

Ore textures primarily include crystalline, metasomatic, exsolution, and compressed textures. Among them, the crystalline and metasomatic textures are the main ore-forming types. The main characteristics of these textures are as follows.

Idiomorphic granular textures: textures of this type are primarily present in swiftly growing pyrite, which predominantly occurs as cubic crystals, followed by pentagonal dodecahedral crystals, with streaks on the crystal faces. Disseminated pyrite frequently displays this type of textures.

Hypidiomorphic granular textures: textures of this type are also primarily present in pyrite, followed by ilmenite and marcasite. Disseminated and veined pyrite mainly shows hypidiomorphic or idiomorphic granular textures.

Anhedral granular textures: textures of this type develop in many minerals, such as magnetite, pyrrhotite, chalcopyrite, tetrahedrite, and sphalerite, usually occurring as aggregates.

Foliaceous or scaly textures: textures of this type are unique to molybdenite, usually exhibiting a directional arrangement. Large molybdenite shows foliaceous textures, while small molybdenite presents scaly textures, mostly occurring as aggregates.

Tabular texture: textures of this type develop in some molybdenite and accessory minerals formed by magma crystallization, such as ilmenite. These minerals, exhibiting anhedral to hypidiomorphic tabular textures, mostly occur as aggregates.

Chrysanthemum petal-like textures: textures of this type are uncommon, also developing exclusively in molybdenite. Foliaceous or scaly molybdenite often forms radial aggregates, presenting textures similar to chrysanthemum petals. These textures, with diameters of 0.5–5 mm, are frequently visible in wide quartz veins and pegmatoid veins formed in the early stage.

Poikilitic textures: textures of this type are common, primarily manifested as pyrite wrapping chalcopyrite, pyrrhotite, or ilmenite. These textures result from the minerals crystallized early being trapped by those formed late.

Metasomatic relict textures: textures of this type are common, primarily forming by the metasomatic replacement of ilmenite, chalcopyrite, sphalerite, and pyrrhotite by pyrite; the metasomatic replacement of pyrite by tetrahedrite and chalcopyrite, and the metasomatic replacement of ilmenite by molybdenite. The incomplete metasomatism leads to the

formation of metasomatic relict textures.

Skeleton textures: textures of this type are very rare, manifested mainly as pyrite metasomatizing ilmenite and appearing as the tabular pseudomorphs of ilmenite.

Exsolution textures: textures of this type are also very rare, usually in a droplet shape. In other words, droplet-shaped chalcopyrite is wrapped in sphalerite, or sphalerite is wrapped in chalcopyrite grains, indicating that they were miscible at high temperatures and then the solid solution phase unmixed as the temperature dropped, forming immiscible paragenetic structures. When the temperature dropped swiftly, the solid solution phase was unmixed quickly, and accordingly, the precipitates formed droplet-shaped textures before migrating and aggregating.

Cataclastic textures: early-crystallized pyrite became cataclastic under the action of late dynamic effects, thus forming cataclastic textures. Occasionally, relative displacement occurs along the crushed fissures, and the resultant interstices are frequently filled with other metallic minerals.

Crumpled textures: foliaceous molybdenite is subjected to bending deformation rather than crushing under the action of dynamic effects, thus forming crumpled textures, which tend to be characterized by wavy extinction.

4.2.3. Ore structures

The ore structures primarily comprise veined and veinlet-disseminated structures, followed by disseminated structures, as well as brecciated and lumpy structures.

Disseminated structures: the structures of this type, which are widespread and dominated by sparse disseminated structures, are unevenly distributed. In these structures, metallic minerals such as molybdenite, pyrite, ilmenite, and chalcopyrite occur as monocrystals or aggregates. These minerals have grain sizes generally less than 0.5 mm, except for some pyrite, which has a grain size of 2 mm. Generally, the structures of this type indicate the ore-forming fluids with high temperatures and concentrations and ores with high effective porosities and permeabilities, which are conducive to infiltration metasomatism.

Veined structures: the structures of this type, which are the most important structures of ores, were formed by metal sulfide minerals and gangue minerals, such as quartz, in various micro-faults and fractures. Generally, these structures exhibit straight vein walls and clear boundaries. They roughly reflect that ore-bearing rocks host fractures, where the filled ore-forming fluids exhibited a decreased temperature. The metallic minerals in veins primarily include molybdenite and pyrite, followed by ilmenite, chalcopyrite, sphalerite, and galena. There are three mineralization patterns, and the details are as follows: (1) extremely fine-grained molybdenite is evenly distributed in quartz veins in dust form, exhibiting gray veins. This mineralization pattern is termed vaporific molybdenite mineralization. (2) Slightly larger-grained molybdenite tends to be directionally distributed on vein walls or within quartz veins, forming roughly parallel intermittent thin strips. These thin strips are relatively developed at veins edges and gradually diminish towards the central part. (3) Pure sulfide mineral veinlets consist primarily of molybdenite and pyrite. Vein structures can be divided into broad-vein, veinlet, and micro-vein structures with vein widths of > 10 mm, 1–10 mm, and < 1 mm, respectively. Most of them are veinlet structures. Molybdenum mineralization in broad veins tends to appear as aggregates or lumps, while micro-veins primarily form by the penetration of relatively pure molybdenite along small fractures. As a result, molybdenite fills are commonly visible on fracture surfaces. Occasionally, molybdenite or pyrite veinlets penetrate into molybdenum-bearing quartz veins, forming complex veined structures. When multiple sets of fractures develop and ore-bearing veins intersect with each other, a stockwork structure is formed.

Veinlet-disseminated structures: when multiple sets of ore-bearing veins intersect with each other, some disseminated mineralization tends to occur nearby, thus forming veinlet-disseminated structures. The structures of this type reflect the diffusive metasomatism of the surrounding rocks by ore-bearing hydrothermal fluids as the fluids penetrated and filled into fractures. In particular, disseminated molybdenum mineralization is more prone to form in intergranular pores of sericite near veins. In addition, veinlet-disseminated structures can also be formed by the superimposition of veined and disseminated structures. As a main structural type of ores, veinlet-disseminated structures are widely distributed, especially in high-grade ores.

Brecciated structures: the structures of this type are visible in structurally fractured zones and cryptoexplosive breccia pipes. They can be divided into three types according to the compositions of breccias and cements: (1) Ores and ore-bearing veins are fractured into breccias, and cements primarily include hydrothermal alteration materials such as lithic fragments, hydromuscovite, quartz, and carbonate; (2) Rocks are fractured into breccias, and cements consist mainly of quartz, molybdenite, pyrite, and sericite. These breccias are mostly cut through by molybdenum-bearing quartz veins; (3) Breccias are produced from the fracture of both rocks and molybdenum-bearing quartz veins, and their cements contain both metallic sulfides, such as molybdenite and pyrite, and altered minerals, such as quartz, hydromuscovite, and hydromica. Brecciated structures are of great significance for ore origin, indicating that the Daheishan deposit underwent multiple tectonic activities during its metallogenic process and was subjected to cryptoexplosion after the dominant mineralization period.

Lumpy structures: pyrite in the form of lumpy aggregates is distributed in quartz veins or rocks, forming lumpy structures. These structures are rare, especially lumpy molybdenite.

4.3. Alteration and zoning of surrounding rocks

The ore-bearing plutons in the Daheishan deposit generally underwent hydrothermal alteration, which can be divided into two periods. The first period, associated with granodiorite porphyries, is the most closely related to

mineralization. The second period, associated with felsitic granodiorite porphyries, represents the superimposed alteration following the dominant mineralization period. The alteration types primarily include K-feldspar alteration, biotite alteration, silicification, sericite alteration, muscovite alteration, hydromuscovite alteration, kaolin alteration, zeolite alteration, and carbonation. The two periods of alterations are superimposed and can be roughly divided into five alteration zones, as follows (Fig. 7).

4.3.1. Quartz-K-feldspar alteration zone

The quartz-K-feldspar alteration zone, which is the earliest alteration zone in the mining area, was formed by the superimposition of various altered rocks with three alternation types, namely K-feldspar, quartz-K-feldspar, and biotite-quartz-K-feldspar alterations. The altered rocks in this alteration zone are distributed in granodiorite porphyry plutons and inequigranular granodiorite plutons in outer contact zones. In a planar view, this alteration zone exhibits a subcircular distribution pattern with granodiorite porphyries as the center. Vertically, it gradually contracts from the alteration zone's edge near the surface to the deeper part of the center of the granodiorite porphyries. This alteration zone exhibits uneven alteration intensity, which is high in the upper and interior parts and low in the lower and edge parts. The altered mineral assemblages in the strongly altered sections of this alteration zone primarily show an areal distribution pattern, while the weakly altered sections predominantly present linear alterations distributed as sparse veins. Occasionally, alternating strong and weak alterations are distributed in some sections. Due to the superposition of later alterations, this alteration zone transitions into beresite and quartz-sericite alteration zones inward and outward, respectively. In the deeper part, the exterior of this alteration zone transitions directly into the propylite alteration zone.

4.3.2. Quartz core-stockwork zone

The quartz core-stockwork zone is composed primarily of granodiorite porphyries subjected to strong quartz alteration. This zone is characterized by dense quartz stockworks and several large-scale quartz-pegmatoid veins with lengths of 150–300 m and widths of 20–50 m, which form the nearly-WE-directed quartz core. These wide veins are surrounded by granodiorite porphyry breccias, indicating that they were formed by filling and metasomatism along tectonic weak zones. Late alteration superposition led to extensive sericite alteration on the joint and fracture surfaces of the veins. Furthermore, the pegmatoid K-feldspar and surrounding rock breccias within the veins were all metasomatized by late quartz and sericite. This zone, deviating from the center of the granodiorite porphyry plutons, is positioned in the middle-upper part of the southern branch of the granodiorite porphyry plutons distributed in the southeast of the Daheishan deposit. With a small outcrop area, this zone transitions to the quartz-sericite alteration zone outward. The large quartz-pegmatoid veins, with originally slight molybdenum mineralization, exhibit moderately to weakly molybdenum mineralization due to the superposition of the quartz-sericite alteration and ore-bearing quartz veins.

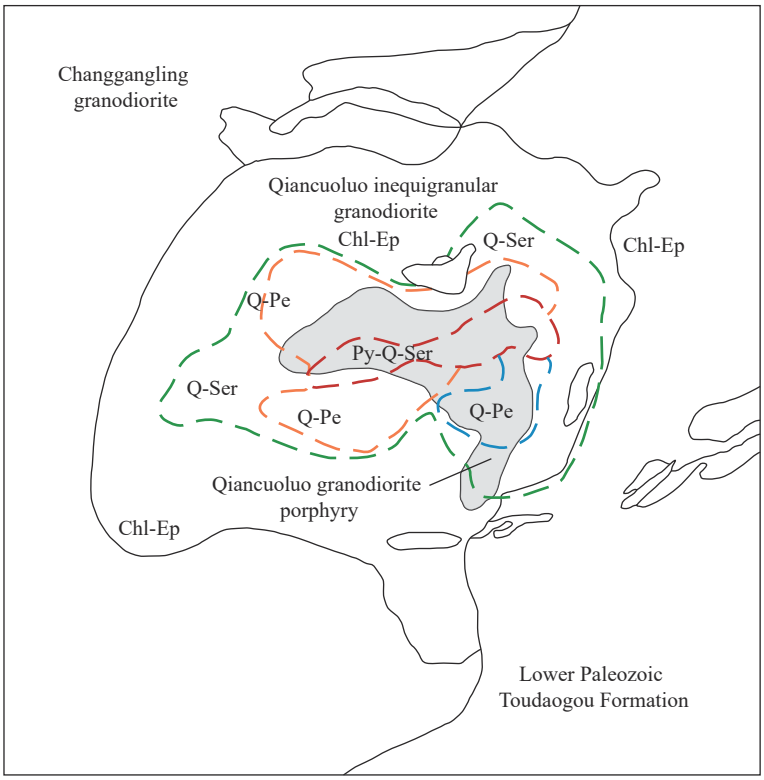

Fig. 7. Sketch map of alteration zones in the Daheishan molybdenum deposit (after Lu ZQ, 2017). Chl-Ep: propylitization; Q-Ser: quartz-sericitization; Q-Pe: potassium feldspathization; Py-Q-Ser: ferrosericitization; Q-ρe: quartz core-quartz veins.

4.3.3. Quartz-sericite alteration zone

The quartz-sericite alteration zone is distributed in a ringlike pattern around the quartz-K-feldspar alteration zone and the quartz core-stockwork zone. This alteration zone, exhibiting stronger alternation in the eastern part of the mining area than in the western part of the area, extends into the metamorphic intermediate-mafic volcanic rocks of the Toudaogou Formation. It extends shallowly downward, with the extension not exceeding the elevation of 0 m. This alteration zone is formed by the metasomatism of different protoliths by veined or zonal alteration veins of sericite hydromuscovite and quartz-sericite hydromuscovite. An alteration zone with 10% or more of the above-mentioned veins can be classified as a quartz-sericite alteration zone. The altered protoliths predominantly comprise inequigranular granodiorites, followed by granodiorite porphyries, metamorphic intermediate-mafic volcanic rocks, and metasandstones. The exterior of this alteration zone transitions into the propylite alteration zone.

4.3.4. Beresite alteration zone

The beresite alteration zone is mainly housed in the middle-upper part of the granodiorite porphyry plutons. In a planar view, this alteration zone displays a nearly-W-E-directed zonal distribution pattern in a narrow range. Similar to the outcrop range of molybdenum-rich ore bodies, this alternation zone is located in the center of horizontal alteration zones. The south and north sides of this alteration zone transition to the quartz-K-feldspar alteration zone, and the east and west sides transition to the quartz-sericite alteration zone. In the center of the upper part of this alteration zone, sericite, hydromuscovite, and pyrite, which are paragenetic, metasomatized granodiorite porphyries planarly, gradually presenting a zonal or veinlet distribution towards the surrounding beresite. As the alteration intensity weakens, the altered veins show gradually decreased occurrence frequency and vein widths. Generally, an alteration zone with more than 10% of altered veins can be classified as a beresite alteration zone. This alteration zone, which is superimposed on the quartz-K-feldspar alteration zone, exhibits some residual quartz-K-feldspar altered rocks formed early between beresite bands. This alteration zone has a vertical depth of over 300 m and transitions to the quartz-K-feldspar alteration zone.

4.3.5. Propylite alteration zone

The propylite alteration zone, which is the outermost alteration zone of the Daheishan deposit, is distributed around granodiorite porphyries. This alteration zone is composed of altered rocks subjected to propylite alteration, such as inequigranular granodiorites, granodiorite porphyries, metamorphic intermediate-mafic volcanic rocks, and metasandstones. It covers a wide distribution range, reaching 1–2 km away from the center of the Daheishan deposit. Propylite alteration within plutons is evidenced by varying degrees of chlorite alteration and weak epidote alteration of primary biotite, as well as the weak clay alteration and carbonation of plagioclase, with some plagioclase showing decalcification-induced oligoclase-albite alteration of clear rims. The propylite alteration of the metamorphic intermediate-mafic volcanic rocks and metasandstones in the Toudaogou Formation is mainly manifested as follows: the irregular veinlets of chlorite and a minor amount of epidote are filled and metasomatized along rock joints and fractures or distributed along both sides of quartz veinlets. Compared to the typical propylite alteration, the propylite alteration in the mining area of the Daheishan deposit is relatively weak.

The developmental degrees and spatial distribution of various alteration zones in the mining area are closely related to granodiorite porphyries, resulting from the superposition of gas-liquid and hydrothermal alteration stages after the mineralization period of granodiorite porphyries. In combination with the alteration mechanisms of ore-bearing hydrothermal fluids, this study proposes that the alteration zoning in the Daheishan deposit has the following characteristics: with granodiorite porphyries as the center, the alteration zones consist of beresite, quartz-K-feldspar, quartz-sericite, and propylite alteration zones outward. The quartz-K-feldspar alteration zone, formed in the gas-liquid alteration stage, and the quartz-sericite alteration zone, formed in the early hydrothermal alteration stage, exhibit a gradual transition pattern, constituting the main alteration model in the Daheishan deposit. In the early stage, the quartz-K-feldspar alteration was extremely developed and widespread, especially in the upper-central part of the quartz-K-feldspar alteration zone, on which the beresite alteration zone under the control of W-E-oriented fracture zones is superimposed. A quartz core deviating from the mineralization center exists in the upper part of the granodiorite porphyries. In the late stage, epithermal alteration, such as carbonation and zeolite alteration, formed and was superimposed on various alteration zones. However, epithermal alteration is intense in the moderately deep part of the quartz-K-feldspar alteration zone and in the quartz-sericite alteration zone but weak in the beresite alteration zone.

Based on the alteration of the Kalamazoo deposit and data on 27 porphyry copper/molybdenum deposits in America, Shan WL et al. (1991) proposed the alteration model of porphyry copper/molybdenum deposits, which is consistent with the alteration model of the Daheishan deposit.

4.4. Mineralization periods and stages

The Daheishan deposit is the result of ore-bearing hydrothermal fluids acting on rocks. The entire alteration and mineralization process witnessed the evolution of ore-bearing hydrothermal fluids. Based on this, the Daheishan deposit has two main mineralization periods: the hydrothermal mineralization period and the supergene mineralization period (Table 5).

4.4.1. Hydrothermal mineralization period

During this period, the ascending ore-bearing

Table 5. Mineralization stages and mineral generation sequence of the Daheishan molybdenum deposit (after Wang ZG, 2012).

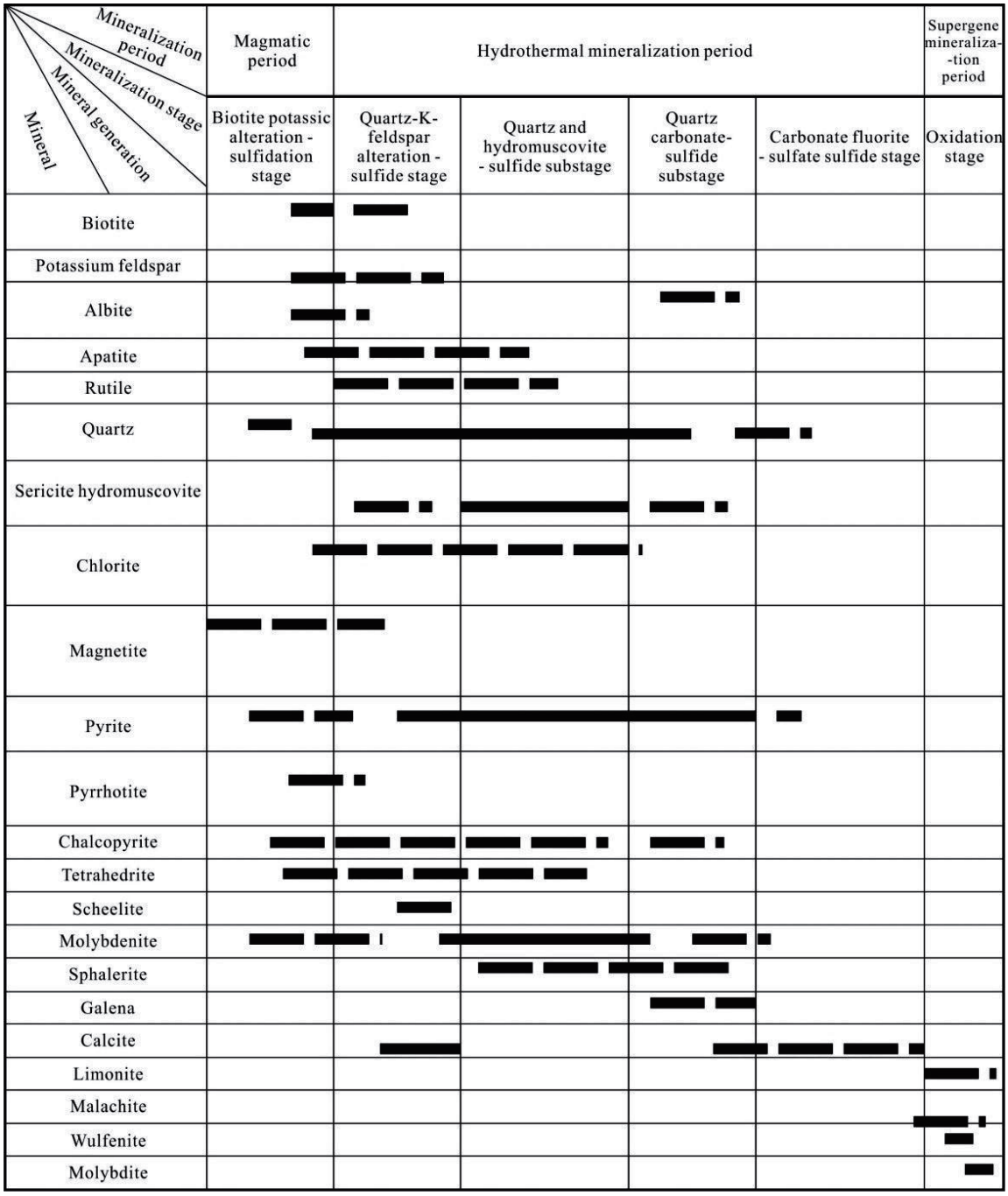

hydrothermal fluids began to mix with groundwater. Based on the changes in the physical and chemical conditions of ore-bearing hydrothermal fluids, as well as the paragenetic and combination relationships of hydrothermal minerals, this hydrothermal mineralization period can be divided into four mineralization stages:

Quartz-magnetite stage: with the emplacement of porphyry magmas, the ore-bearing hydrothermal fluids rose and then reacted with rocks, forming potassic-alteration rocks composed of altered minerals such as biotite, K-feldspar, and quartz in the early stage. In the process of potassic metasomatism, H_2S appeared in the ore-bearing hydrothermal fluids as the temperature continuously decreased. The combination of H_2S with metal elements led to the formation of metal mineralization, such as early disseminated magnetite and pyrrhotite, which are scattered in rocks. The alteration at this stage was dominated by veined penetration, forming extensive quartz-K-feldspar veinlets and pegmatoid veins. These veins penetrated the early-formed rocks subjected to biotite-quartz-K-feldspar alteration. Furthermore, disseminated molybdenite, pyrite, and chalcopyrite were formed along with the alteration.

Quartz-pyrite-molybdenite stage: at this stage, the ore-bearing hydrothermal fluids, still dominated by deep-source ore-bearing gas and liquids, were mixed with some groundwater and thus gradually became mixed ore-forming

liquids. Large amounts of hydromuscovite and sericite were formed by the hydrolyzation of plagioclase and K-feldspar. As a major feature of this stage, the oversaturation of silica in the hydrothermal fluids led to strong quartz-sericite alteration, as well as beresite alteration characterized by the combination of pyrite, hydromuscovite, sericite, and quartz. Subsequently, H_2S was hydrolyzed by SO_2 as the temperature decreased. Then, H_2S was combined with metal elements in the hydrothermal fluids, leading to the precipitation of large quantities of metal sulfide minerals such as molybdenite, pyrite, chalcopyrite, and sphalerite. These metal sulfide minerals filled fractures as molybdenum-bearing quartz veins, pyrite-molybdenite-quartz veins, and pyrite-quartz veins mostly, causing strong molybdenum mineralization. In the late stage of the molybdenum mineralization, molybdenite or pyrite veinlets with few gangue minerals frequently penetrated along fractures owing to the further concentration of sulfur and metal ions in the ore-forming fluids, as well as appropriate physical and chemical conditions such as temperature, pressure, and pH. This mineralization stage, witnessing the formation of large-scale molybdenum ore bodies, is the most significant mineralization stage of the mining area. It is noteworthy that the mineralization at this stage involved multiple mineralization processes, which were superimposed on the middle-upper parts of ore bodies, leading to the formation of high-grade ore blocks. The fractures remained open, providing conditions for multiple filling of ore-forming fluids.

Overall, the molybdenum-bearing quartz veins widened and the grain sizes of molybdenite increased from early to late at this stage. In addition, the sequence of alteration and mineralization at this stage can be verified by the cross-cutting relationships of various veins.

Quartz-polymetallic-sulfide stage: at this stage, a large amount of groundwater entered and dominated the ore-bearing hydrothermal fluids, making the fluids neutral to slightly alkaline. This stage witnessed the formation of pyrite, chalcopyrite, bornite, sphalerite, galena, molybdenite, and quartz veins. Among them, quartz veins showed an uneven ore distribution, with pyrite and molybdenite veins concentrated in local sections.

Quartz-carbonate stage: at this stage, the ore-bearing fluids had already evolved into low-temperature (below 200°C) hydrothermal fluids dominated by groundwater, with very low concentrations of metal ions and only a small amount of crystallized pyrite. This stage witnessed the formation of calcite-fluorite, calcite-zeolite, and quartz veins, which were very clean and bore rare metal sulfides. After this stage, the whole hydrothermal activity ended.

4.4.2. Supergene mineralization period

The Daheishan deposit exhibited very weak supergene mineralization and the absence of secondary enrichment, with small amounts of secondary oxides, such as molybdite, malachite, and limonite, only visible near the surface. Therefore, the supergene mineralization period of the Daheishan deposit has no industrial significance.

4.5. Resources and ore chemical composition of the Daheishan deposit

IntheDaheishandeposit,theprimarymineral—molybdenum—has an average grade of 0.081%, and the associated minerals copper, sulfur, gallium, and rhenium have average grades of 0.033%, 1.67%, 0.001%, and 0.0012%, respectively. To date, the remained mineral resources of the deposit within the mineral right are as follows: for molybdenum, remained ore content: 234933 kt, metal content: 189849 t, average grade: 0.081%; for sulfur, ore content: 234933 kt, sulfur content: 3923381 t, average grade: 1.67%; for copper, ore content: 234933 kt, metal content: 77258 t, average grade: 0.033%; for gallium, ore content: 234933 kt, metal content: 2349 t, average grade: 0.001%; for rhenium, ore content: 189849 t, metal content: 2 t, average grade: 0.0012% (Shi ZY et al., 2008; Wang ZG, 2012). The cumulative proven mineral resources are as follows: for molybdenum, ore content: 264899 kt, metal content: 215510 t, average grade: 0.081%; for sulfur, ore content: 264899 kt, sulfur content: 4423813, average grade: 1.67%; for copper: ore content: 250260 kt, metal content: 81469 t, average grade: 0.033%; for gallium, ore content: 264899 kt, metal content: 2649 t, average grade: 0.001%; for rhenium, ore content: 215510 t, metal content: 3 t, average grade: 0.0012% (Wang ZG, 2012).

Wang L (2012) analyzed the chemical composition of ore samples, concluding that the significantly varying contents of major oxides in the Daheishan deposit are related to the different types and intensities of hydrothermal alteration (Table 6). In sections with strong quartz-K-feldspar and quartz-sericite alterations, the K_2O, SiO_2, and H_2O contents increase to varying degrees, while the FeO, Fe_2O_3, MgO, Al_2O_3, and TiO_2 contents decrease. The industrial ore bodies of the deposit are located in the superimposed position of K-feldspar, quartz-sericite, and beresite alterations. Accordingly, they exhibit strong alteration, with average SiO_2 and K_2O contents being 14% and 16.26% higher than those of low-grade ores, respectively. The ores have a single useful component —molybdenum. The main associated useful component is sulfur, with contents varying in the range of 0.24%–2.70% and an average grade of 2.00%, meeting the standards for comprehensive utilization. Other beneficial elements, such as Cu, Ga, Re, Au, and Ag, fall below the standards for comprehensive utilization. However, Cu, with an average grade of 0.033%, was recycled and utilized due to the improved beneficiation process and was included in the estimation of resources and reserves.

5. Discussion

5.1. Mineralization epoch

The age of mineralization for the Daheishan deposit has been a point of study and contention for several researchers. Some researchers determined the K-Ar isotopic age of biotite

in the Daheishan plutons at 354 Ma, which, however, is deemed unreliable due to the influences of hydrothermal fluids and late-stage alterations. Several other studies have produced different age estimates (Table 7). For example, Ge WC et al. (2007) determined the zircon U-Pb ages of ore-free monzogranites and ore-bearing granodiorite porphyries in the deposit to be 178±3 Ma and 170±3 Ma, respectively. Zhou et al. (2014) determined the ages of early Changgangling biotite granites to be 177.9±2.3 Ma and the ages of late Qiancuoluo biotite granodiorites and granodiorite porphyries to be 169.9±3.2 Ma and 167.6±4.0 Ma, respectively. These two sets of ages roughly align with the findings of Ge WC et al. (2007). In addition, through Re-Os isotopic dating, Wang CH et al. (2009) determined the ages of 10 molybdenite samples with different attitudes collected from the Daheishan mining area, obtaining their model ages of 168.1–169.1 Ma and Re-Os isochron age of 168.2±3.2 Ma. Zhang et al. (2015) found the Re-Os age of a single molybdenite sample to be 167.2 Ma, which, combined with the age data obtained by Wang CH et al. (2009), constituted an isochron age of 168.7±3.1 Ma. The isochron age of molybdenite obtained by Zhou et al. (2014) is also the Middle Jurassic (171±8 Ma), which is consistent with the two groups of ages mentioned above within the error range. The formation age of ore-bearing granites aligns with the crystallization age of molybdenite within the error range, indicating that the Daheishan deposit was formed during the Middle Jurassic (170–168 Ma). Zhou LL et al. (2014) determined the Ar-Ar age of muscovite, obtaining a plateau age of 163.6±0.9 Ma, which is believed to represent the end time of magmatic activity or late hydrothermal activity, or in other words, the age of the final mineralization stage (Chen JS et al., 2015). According to Lu ZQ (2017), monzogranite samples had zircon U-Pb isotopic ages of 180±2–177±2 Ma, with a weighted average of 178.4±0.9 Ma [mean square weighted deviation (MSWD)=0.20], representing the formation age (Early Jurassic) of monzogranites in the Daheishan deposit. Furthermore, granodiorite porphyry samples had zircon U-Pb isotopic ages of 172±3–167±2 Ma, with a weighted average of 169.9±0.9 Ma (MSWD=0.41), representing the formation age (Middle Jurassic) of granodiorite porphyries in the Daheishan deposit (Lu ZQ, 2017). All these results lead to the conclusion that the formation and mineralization ages of the Daheishan deposit should be earlier than 164 Ma, corroborating that the Daheishan deposit was formed during the Middle Jurassic and experienced the Early Yanshanian mineralization (Hou XG, 2017).

Many researchers are interested in the diagenetic and metallogenic epochs of molybdenum deposits, including the Daheishan deposit in central Jilin. They have obtained many new insights and abundant data through geochronological research (Sun SS et al., 1989; Sun FY et al., 2000; Ge WC et al., 2007; Wang CH, 2009; Ju N et al., 2012; Zhang Y, 2013). The following summary presents the research results about the diagenetic and metallogenic epochs of representative porphyry molybdenum deposits in this area (Table 8).

Table 6. Contents of major chemical elements in ores of the Daheishan molybdenum deposit (after Wang L, 2012).

Element	Content/%		Element	Content/%		Element	Content/%	
	Average	Range		Average	Range		Average	Range
O	48.41	40.08–60.84	H	0.144	0.051–0.517	Pb	0.0044	0.0003–0.35
Si	32.26	28.33–34.36	Cl	0.12	0.01–0.28	W	0.0042	0.00031–0.06
Al	7.79	6.77–11.47	P	0.059	0.022–0.11	As	0.00179	0.0002–0.02
K	4.17	1.33–7.47	Mo	0.049		Ga	0.00156	0.0005–0.003
Fe	2.23	0.58–5.50	Ba	0.044	0.003–0.25	Ni	0.00088	0.0005–0.0024
Na	1.98	0.26–3.29	Sr	0.038	0.0025–0.1395	Co	0.000654	0.0002–0.001
Ca	1.33	0.20–2.19	Cr	0.0304	0.001–0.08	Sn	0.000595	0.0002–0.0025
S	1.67	0.24–2.70	Cu	0.029		Ag	0.000074	0.000005–0.002
Mg	0.46	0.05–0.90	Mn	0.023	0.008–0.054	Re	0.00006	0–0.00014
Ti	0.27	0.19–0.42	Zn	0.0159	0.001–0.9	Ru	0.0000001	0.0000001
C	0.197	0.08–0.44	Rb	0.0144	0.0007–0.0324	Au	0.01g/t	0.00000002–0.00000018
F^-	0.16	0.04–0.40	V	0.006	0.002–0.015			

Table 7. Statistics of diagenetic and mineralization ages of the Daheishan molybdenum deposit (after Hou XG, 2017).

Test subject	Isotopic age/Ma	Dating method	Data source
Ore-free monzogranite	178±3	SHRIMP zircon U-Pb dating	Ge WC et al., 2007
Changgangling biotite granite	177.9±2.3	LA-ICP-MS zircon U-Pb dating	Zhou LL et al., 2014
Qiancuoluo biotite granodiorite	169.9±2.3	LA-ICP-MS zircon U-Pb dating	Zhou LL et al., 2014
Qiancuoluo granodiorite porphyry	167.6±4.0	LA-ICP-MS zircon U-Pb dating	Zhou LL et al., 2014
Ore-bearing granodiorite porphyry	170±3	SHRIMP zircon U-Pb dating	Ge WC et al., 2007
Molybdenite	168.2±2.3	Molybdenite Re-Os dating	Zhang Y et al., 2013
Molybdenite	168.7±3.1	Molybdenite Re-Os dating	Zhou LL et al., 2014
Molybdenite	171±8	Molybdenite Re-Os dating	Zhou LL et al., 2014
Muscovite	163.6±0.9	Ar-Ar isotopic dating of molybdenite	Zhou LL et al., 2014

Li BL et al. (2009) conducted Re-Os isotopic dating of five molybdenite samples from the Fu'anpu molybdenum deposit. The results showed that molybdenite samples had Re content of 9.94×10^{-6}–15.12×10^{-6}, model ages of 165.3±2.4–167.0±2.3 Ma (average: 166±1.0 Ma), and an isochron age of 166.9±6.7 Ma, with an MSWD of 0.60. Accordingly, they concluded that the Fu'anpu deposit formed during the Early Yanshanian. Yu XQ et al. (2008) also conducted Re-Os isotopic dating of eight molybdenite samples from the Fu'anpu deposit, obtaining model ages of 166.9–169.9 Ma, a weighted average of 168.22±0.87 Ma, and an isochron age of 171±3 Ma. Therefore, they drew the same conclusion about the formation age of the Fu'anpu deposit. Through zircon U-Pb isotopic dating, Liu B (2001) determined that the porphyroid monzogranites (ore-hosting surrounding rocks) of the deposit have a weighted average age of 179±2 M. Similarly, Zhang Y (2013) conducted the zircon U-Pb isotopic dating of porphyroid monzogranites and migmatitic granites in the Fu'anpu deposit, obtaining weighted average ages of 167.05±0.81 Ma and 170.42±0.91 Ma, respectively. All these results indicate that the Fu'anpu molybdenum deposit is the product of the Early Yanshanian metallogenic event.

Zhang Y (2013) tested four granodiorite samples from the ore-forming plutons of the Jidetun deposit, obtaining single-grain zircon U-Pb ages of 175.7–168.2 Ma, a weighted average Re-Os isotopic age of 165.9±1.2 Ma, and an isochron age of 168±2.5 Ma. Shao JL et al. (1990) found that the molybdenite samples from the Jidetun molybdenum deposit had Re-Os isotopic model ages of 168.79±0.42–169.91±0.47 Ma, a weighted average age of 169.31 Ma, and an isochron age of 169.1±1.8 Ma (MSWD=7). These similar mineralization ages indicate that the Jidetun molybdenum deposit was formed during the Early Yanshanian.

Wang CH et al. (2009) tested 10 molybdenite samples from the Daheishan deposit, obtaining Re-Os isotopic model ages of 166.9–169.6 Ma and an isochron age of 168.2±3.2 Ma. For granodiorite porphyries closely related to mineralization and granodiorites unrelated to mineralization in the Daheishan deposit, Ge WC et al. (2007) obtained the sensitive high-resolution ion microprobe (SHRIMP) zircon U-Pb ages of 170±3 Ma and 178±3 Ma, respectively. Zhang Y (2013) determined the Re-Os isotopic model age of molybdenite in the deposit to be 168.7±3.1 Ma. Ju N (2020) determined that biotite monzogranites in the Chang'anpu copper/molybdenum deposit have an average zircon U-Pb age of 182.10±1.20 Ma. Therefore, it can be inferred that the Daheishan deposit was formed during the Early Yanshanian.

Ju N et al. (2012) dated the Re-Os isotopic ages of five molybdenite samples from shallow ore bodies of the Dashihe deposit, obtaining model ages of 182.1±2.7–191.9±2.6 Ma, a weighted average age of 186.7±5.0 Ma, and an MSWD of 11.8. Sun DY et al. (2011) determined that the molybdenites in the Dashihe deposit have a Re-Os isotopic model age of 185.6±2.7 Ma. The two groups of data are roughly consistent, indicating that the Dashihe molybdenum deposit formed during the Early Yanshanian.

As revealed by the above metallogenic chronological research, the metallogenic events of molybdenum deposits represented by Daheishan and Chang'anpu in central Jilin primarily occurred during the Middle Jurassic. These metallogenic processes occurred almost simultaneously, indicating that the metallogenic process in the late stage of the Early Jurassic or the early stage of the Middle Jurassic occurred in the same geodynamic setting. It is noteworthy that for most molybdenum deposits such as Daheishan, Fu'anpu, and Chang'anpu, the U-Pb ages of ore-bearing porphyry plutons are nearly consistent with the Re-Os ages of molybdenite in ores, indicating that porphyry plutons are more likely to be ore-forming plutons. However, for some molybdenum deposits such as Jidetun and Dashihe, the U-Pb ages of ore-bearing porphyry plutons deviate from the Re-Os ages of molybdenite by more than 5–10 Ma, indicating that the mineralization of molybdenum was later than the diagenetic age of ore-bearing porphyry plutons, and thus the

Table 8. Statistics of the diagenetic and mineralization ages of porphyry molybdenum deposits in central Jilin (after Ju N, 2020).

Number	Deposit	Sample/dating method	Age/Ma	Sample quantity	Data source
1	Daheishan	Molybdenite Re-Os dating	168.2±3.2	10	Wang CH, 2009
		Molybdenite Re-Os dating	168.7±3.1		Zhang Y, 2013
		Zircon U-Pb dating	170±3		Ge WC et al., 2007
		Molybdenite Re-Os dating	169.8±2.4		Zhou LL et al., 2014
2	Fua'npu	Molybdenite Re-Os dating	166.9±6.7	5	Li LX et al., 2009
		Molybdenite Re-Os dating	171±3	8	
		Zircon U-Pb dating	179±2		
		Zircon U-Pb dating	167.05±0.81		Zhang Y, 2013
		Zircon U-Pb dating	170.42±0.91		Zhang Y, 2013
3	Jidetun	Zircon U-Pb dating	175.7-168.2		Zhang Y, 2013
		Molybdenite Re-Os dating	168±2.5	4	Zhang Y, 2013
		Molybdenite Re-Os dating	169.1±1.8		
4	Dashihe	Molybdenite Re-Os dating	186.7±5.0	5	Ju N et al., 2012
		Molybdenite Re-Os dating	185.6±2.7		Zhou LL et al., 2014
5	Chang'anpu	Zircon U-Pb dating	182.1±1.2		Ju N et al., 2012
		Molybdenite Re-Os dating	168±6.2	5	
		Zircon U-Pb dating	170.2±1.6		

porphyry plutons are not ore-forming plutons.

5.2. Sources of ore-forming fluids and materials

5.2.1. Properties of ore-forming fluids

Many previous researchers have conducted studies on the ore-forming fluids of the Daheishan deposit. This deposit contains various fluid inclusions, primarily including mono-phase vapor inclusions (V), mono-phase liquid inclusions (L), two-phase vapor-liquid inclusions (L+V), and daughter mineral-bearing three-phase inclusions (L+V+S; Table 9). CO_2 is the main component of fluid inclusions, and the daughter minerals consist of halite, Fe_2CO_3, and Fe_2O_3. The ore-forming fluids belong to a CO_2-H_2O-NaCl system (Zhang Y, 2013). As indicated by the thermometry of fluid inclusions, the Daheishan deposit has high homogenization temperatures of 160°C–417.6°C, salinities of 4.32%–41.05% NaCleqv, and fluid densities of 0.62–1.03 g/cm^3, signifying medium- to high-temperature and medium- to high-salinity fluids (Tang RL et al., 1995; Tu GZ et al., 1988; Zhang Y, 2013). Zhang Y et al. (2013) estimated that the Daheishan deposit had a mineralization depth range of 1.63–4.61 km, which is nearly the same as the results derived by, and Wang Q et al. (2005) and is similar to the mineralization depths of typical porphyry deposits (Fig. 8).

The ore-forming fluid system of the Daheishan deposit exhibited a certain changing pattern from the early and middle mineralization stages to the late mineralization stage, with homogenization temperatures gradually decreasing from 300°C–460°C to 196.5°C–300°C, and salinities shifting from 1.7%–49.92% NaCleqv to 1.7%–7.1% NaCleqv (Table 10). In the early and middle mineralization stages, the two-phase vapor-liquid aqueous inclusions displayed high temperatures and low salinities. In contrast, the daughter mineral-bearing three-phase inclusions exhibited high temperatures and high salinities, similar to the fluid inclusions of magmatic-

Table 9. Characteristics of inclusions in the Daheishan molybdenum deposit (after Lu ZQ, 2017).

Inclusion type	Size/μm	Homogenization temperature/°C	Salinity/ %NaCleqv	Metallogenic pressure /MPa, calculation method	Depth/km	Data source
V+L	6–12	171–398	1.6–19.8	30–100	4	Wang Q et al., 2007
S+V+L	8–16	313–443	37.9–49.8	Isovolumic cross plot		
V+L	5–25	232–397	1–17	8–22	0.83–0.94	Wang ZG et al., 2011
S+V+L	6–10	243–369	34–44	Isovolumic cross plot		
V+L	8–12	196.5–401.3	1.7–7.1	14.5–35.4	1.5–3.5	Wang L et al., 2012
S+V+L	8–16	313.2–440.5	38.71–49.92	Empirical equation		
V+L	3–16	160–417.6	4.48–12.55	16.3–46.1	1.63–4.61	
S+V+L	4–10	320–405	34.43–41.05	Empirical equation		

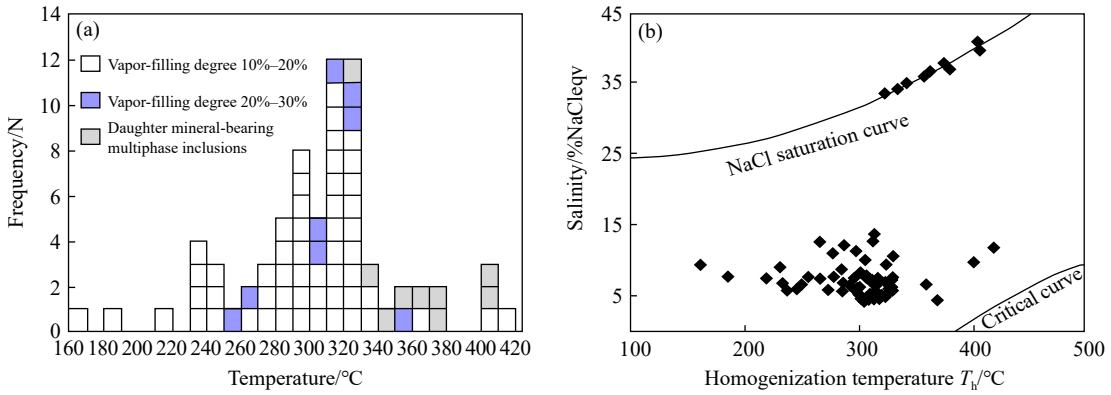

Fig. 8. Histogram and curves of homogenization temperature *vs.* salinity of inclusions in the Daheishan molybdenum deposit (after Zhang Y, 2013).

Table 10. Characteristics and parameters of inclusions in the Daheishan molybdenum deposit (after Zhang Y, 2013).

Mineralization stage	Inclusion type	Size/μm	Gas-liquid ratio/%	Measurement quantity	T_m (ice)/°C	T_h/°C	Salinity /%NaCleqv	Density /g.cm^{-3}	Hydrostatic pressure /MPa	Depth/km
(Ⅰ)	L+V	4–8	10-20	2	−6.5–−8.3	400–417.6	9.8–12	0.65–0.66	41.1–46.1	4.1–4.6
	L+V+S	4–10	20–25	2	–	403–405	39.85–41.05	0.94	39.9–41.1	4–4.1
(Ⅱ)	L+V	3–12	15–25	2	−3.5–−4.7	359–368	4.48–6.58	0.62–0.67	29.9–32.3	3–3.2
	L+V+S	6–10	15–20	5	–	340–378	35–38.16	0.97–1.02	35.8–38.2	3.6–3.8
(Ⅲ)	L+V	5–12	10–20	57	−2.9–9.6	230–340	4.94–13.55	0.73–0.89	20.4–36	2.1–3.6
	L+V+S	6–8	5–15	2	–	320–340	34.43–35.78	1.02–1.03	34.4	3.4
(Ⅳ)	L+V	5–8	5–15	1	−6.5	218	7.43	0.89	20.39	2.04
(Ⅴ)	L+V	4–6	5–15	2	−8.3–12.5	160–185	7.8–9.5	0.93–0.97	16.3–17.6	1.6–1.8

hydrothermal fluids. The coexistence of the two types of inclusions reveals the occurrence of a boiling process. Accordingly, the changes in the physical and chemical conditions of fluids led to large-scale mineral precipitation. In the late mineralization stage, the involvement of meteoric water significantly reduced the temperature and salinity of fluids, forming numerous two-phase vapor-liquid aqueous inclusions with low temperatures and salinities. The ore-forming fluids of the Daheishan deposit, which were high-temperature and high-salinity magmatic fluids in the early stage evolved into the coexisting high-temperature, high-salinity inclusions and high-temperature, low-salinity inclusions in the middle stage under the effects of decompressional boiling or immiscibility and finally into medium- to low-temperature and low-salinity fluids dominated by meteoric water in the late stage (Fig. 9).

5.2.2. Sources of ore-forming fluids

Wang L (2012) tested the hydrogen and oxygen isotopes in quartz samples from the Daheishan deposit, obtaining slightly varying $\delta^{18}O$ values of 7.9‰–11.1‰ and significantly varying δD values of −46.7‰–71.7‰. The $\delta^{18}O$ values of ore-forming fluids from the Daheishan deposit were calculated using the equation for equilibrium fractionation between minerals (e.g., quartz and calcite) and water, expressed as $\delta^{18}OQ\text{-}\delta^{18}O_{H2O}=3.38\times10^6/T2\text{-}3.4$ (Woodcock et al., 1978; Wei JY,1987; Wu G et al., 2005; Wu et al., 2007). The δD values were directly measured from fluid inclusions in quartz and calcite (Fig. 10). The obtained $\delta^{18}O$ and δD values all fell between the magmatic water and meteoric water lines, closer to the magmatic water line. It is generally recognized that the ore-forming fluids of porphyry copper/molybdenum deposits consist primarily of magmatic

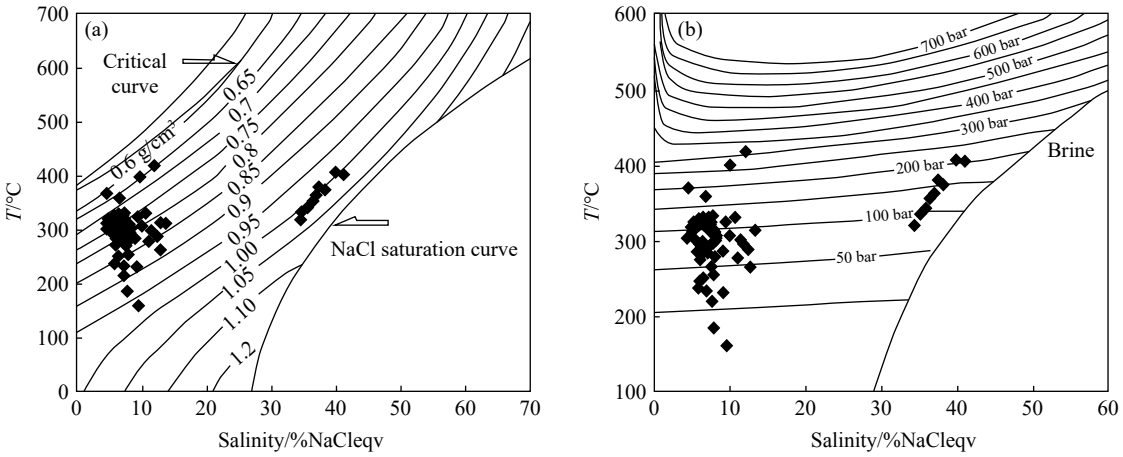

Fig. 9. Diagrams of T-W-ρ (a) and salinity - homogenization temperature - pressure (b) of inclusions in the Daheishan molybdenum deposit (after Zhang Y, 2013).

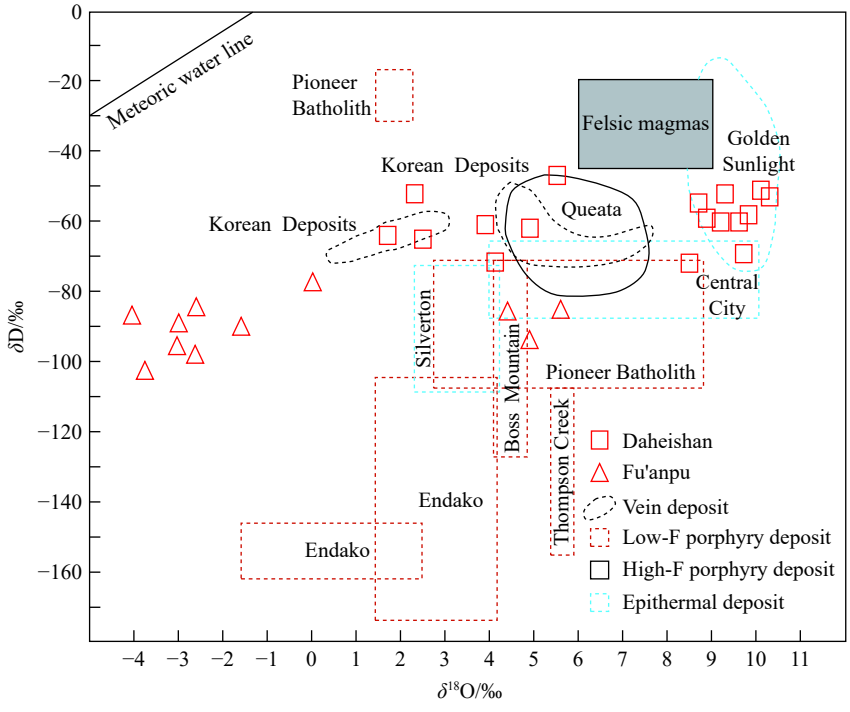

Fig. 10. Projection of hydrogen and oxygen isotopes of the Daheishan molybdenum deposit (after Hou XG, 2017).

water and meteoric water (Rui ZY et al., 1984; Zhu BQ et al., 2001) and that the isotope exchange between magmatic water and ore-forming fluids is the primary reason for the variation in $\delta^{18}O$ values of ore-forming fluids. Therefore, the ore-forming fluids of the Daheishan deposit belong to magmatic water, possibly originating from a deep or even mantle source. Zhou LL et al. (2014) analyzed the hydrogen and oxygen isotopes of quartz veins from various mineralization stages of the Daheishan deposit. The results showed that ore-bearing quartz vein samples had $\delta^{18}O_{H2O}$ values of 8.5‰–10.3‰ and δD values from −72‰ to −51‰. These data primarily fell below the magmatic water line in the δD-$\delta^{18}O$ diagram, far from the meteoric water line. However, the samples from molybdenum-bearing quartz veins in the dominant mineralization of the Daheishan deposit had $\delta^{18}O_{H2O}$ values of 1.71‰–5.51‰ and δD values ranging from −71.7‰ to −46.74‰, which fell significantly closer to the left meteoric water line in the δD-$\delta^{18}O$ diagram (Wang ZG et al., 2012; Zhang Y, 2013). These results reveal that the ore-forming fluids of the Daheishan deposit primarily comprised magmatic water, mixed with a minor amount of meteoric water in the late mineralization stage. Wang YD et al. (1986) tested the oxygen isotopes of different minerals from various mineralization stages of the Daheishan deposit. They found that ore-forming fluids from the quartz-K-feldspar alteration stage, the beresite alteration stage, and the late carbonation stage had average $\delta^{18}Ow$ values of +5.5‰, +2.69‰, and −4.85‰, respectively, indicating the inclusion of meteoric water in the mineralization process. Yu XQ et al. (2008) tested fluid inclusions in ore-bearing quartz veins from the early, main, and late mineralization stages, obtaining homogenization temperatures of 208°C–443°C, 197°C–398°C, and 171°C–301°C and salinities of 2.9%–49.8%, 1.6%–43.9%, and 1.6%–19.8% NaCleqv, respectively. Li T et al. (1963) found that the Daheishan deposit in the main mineralization stage had mineralization temperatures, pressures, and depths of 300°C–390°C, 5–25 MPa, and 0.83–0.94 km, respectively. Determined that the fluid inclusions in the Daheishan deposit had homogenization temperatures of 160°C–417.6°C, salinities of 4.48%–41.05% NaCleqv, $\delta^{18}O$ values of 7.3‰–10.5‰, and δD values of −62‰–−64‰. They concluded that the ore-forming fluids were primarily magmatic water, with the contribution of meteoric water in the later stage.

5.2.3. Sources of ore-forming materials

S isotopes: Wang L (2012) and Zhou et al. (2014) conducted S isotopic analysis of the molybdenite and pyrite in the Daheishan deposit, respectively, obtaining $\delta^{34}S$ values of 0.8‰–2.88‰ (Table 11). Specifically, molybdenite samples had $\delta^{34}S$ values of 1.1‰–2.61‰ (average: 1.94‰), and pyrite samples had $\delta^{34}S$ values of 0.8‰–2.88‰ (average: 1.87‰). All the S isotope values deviated slightly from those of sulfur in meteorites. Moreover, the $\delta^{34}S$ values varied within a narrow range and exhibited a normal distribution roughly. All these indicate highly homogeneous S isotopes and the characteristics of magmatic sulfur. Zhou LL et al. (2014) found that no significant fractionation of S isotopes occurred in various mineralization stages, implying that S isotopes in the Daheishan deposit almost maintain in equilibrium between molybdenite and pyrite. As shown by the analytical results of six ore samples from the Fu'anpu molybdenum deposit, these samples had $\delta^{34}S$ values of 1.5‰–4.1‰, indicating a relatively concentrated distribution of S isotopes; the $\delta^{34}S$ values (1.5‰–1.6‰) of molybdenite were much lower than those (2.6‰–4.1‰) of pyrite, suggesting that the fractionation of S isotopes between molybdenite and pyrite has not yet reached equilibrium (Hou XG, 2017; Fig. 11). Wang ZG (2012) tested the S isotopes of pyrite and molybdenite in ores from the Daheishan deposit. The results demonstrated that the S isotopes in the mining area had high $\delta^{34}S$ values of +0.8‰–+2.5‰ (average: +1.3875), suggesting a slight positive deviation from sulfur in meteorites. The results also showed that the $\delta^{34}S$ values varied slightly and exhibited a prominent tower-like distribution pattern, indicating that S isotopes are highly homogeneous and mainly of mantle origin. These results suggest that ore-forming materials primarily originated from the upper mantle or deep crust (Wang ZG, 2012; Table 12).

Re-Os isotopes: Han CM et al. (2014), Zhou LL et al. (2014), and Wang CH et al. (2009) analyzed the Re-Os isotopes of molybdenite in the mining area, obtaining Re contents of 17×10^{-6}–43.57×10^{-6} (Fig. 12). This result indicates that the ore-forming materials originated from a

Table 11. S isotopic composition of sulfides in ores of typical molybdenum deposits in central Jilin (after Hou XG, 2017).

Deposit name	Sample no.	Tested mineral	$\delta^{34}S_{V\text{-}CDT}$/‰	Data source
	LM01-N12	Pyrite	5.7	
	LM01-12	Molybdenite	4.5	
	LM11-B5	Pyrite	5.1	
	LM11-B14	Pyrite	5.2	
	LM-11-W1	Pyrite	4.5	
	LM-11-W1	Molybdenite	5	
Luming	LM01-B33	Molybdenite	4.5	
	LM-F-1	Molybdenite	5.63	Xia B, 2000
	LM-F-2	Molybdenite	5.54	
	LM-1	Pyrite	6.71	
	LM-20	Molybdenite	5.37	
	LM-21	Molybdenite	5.52	
	LM-30	Molybdenite	5.68	

Table 11 (*Continued*)

Deposit name	Sample no.	Tested mineral	$\delta^{34}S_{V\text{-}CDT}$/‰	Data source
Huojihe	DKH11	Pyrite	1.2	Xiao QH et al., 2002
	DKH12	Pyrite	1.8	
	DKH43	Pyrite	4.2	
	DKH45	Pyrite	4.4	
	DHSTJ4-01-B54	Molybdenite	2.5	Wang L, 2012
	3DHSTJ02-02-B13	Molybdenite	1.9	
	DHSTJ02-03-B3	Molybdenite	1.1	
	DHSTJ4-01-B58	Molybdenite	1.3	
	DHSTJ4-01-B12	Pyrite	1	
	DHSTJ4-01-B38	Pyrite	0.8	
	1DHSTJ02-05-B1	Pyrite	1.3	
	DHSTJ4-01-B17	Pyrite	1.2	
Daheishan	DH-271	Pyrite	1.83	Zhou LL et al., 2014
	DH-258	Pyrite	2.35	
	DH-259	Pyrite	2.52	
	DH-270	Pyrite	2.06	
	DH-263	Pyrite	2.57	
	DH-305	Pyrite	2.07	
	DH-78	Pyrite	2.88	
	DH-301	Molybdenite	2.17	
	DH-254	Molybdenite	1.96	
	DH-255	Molybdenite	2.61	
	DH-261	Molybdenite	2.04	
	DH-272	Molybdenite	1.84	
Fu'anpu	FAP-08	Pyrite	2.6	Xing SW et al., 2005
	FAP-10	Pyrite	4.1	
	FAP-11	Pyrite	2.7	
	FAP-29	Molybdenite	1.6	
	FAP-30	Molybdenite	1.5	
	FAP-31	Molybdenite	3.2	

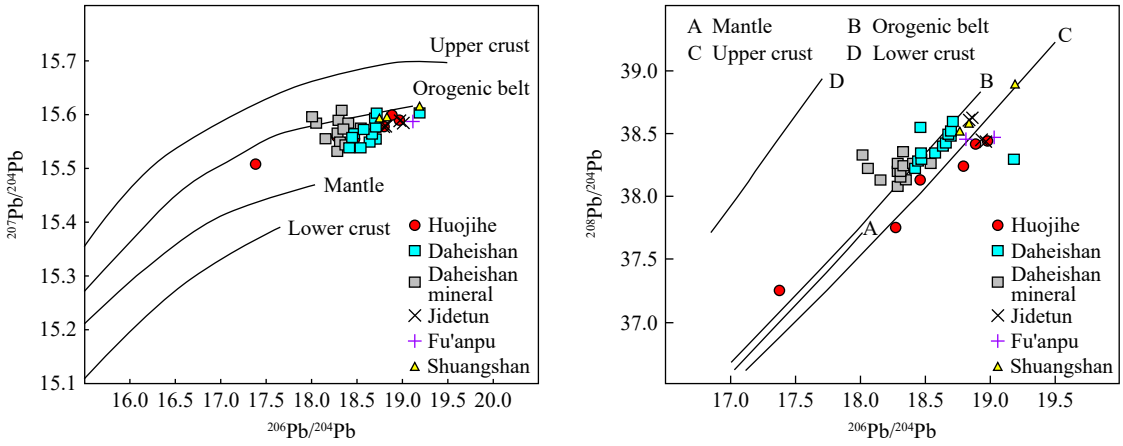

Fig. 11. Pb isotopic characteristics of ore minerals in typical molybdenum deposits in the eastern Jilin-Heilongjiang area (after Hou XG, 2017).

mixed crust-mantle source. The molybdenum deposits in the study area, namely Daheishan, Fu 'anpu, Xinhualong, Liushengdian, Dashihe, Jidetun, Houdaomu, Sifangdianzi, and Tianbaoshan (Dongfeng), have average Re contents of 30×10^{-6}, 11.74×10^{-6}, 61.63×10^{-6}, 15.82×10^{-6}, 6.62×10^{-6}, 0.47×10^{-6}, 48.81×10^{-6}, 4.75×10^{-6}, and 5.01×10^{-6}, respectively (Table 13). These values are generally consistent with the characteristics of molybdenum-dominant porphyry and hydrothermal deposits in foreign countries and areas in China such as the North China Platform and the Qinling Mountains. Moreover, for the molybdenum deposits in the study area, their ore-forming materials originated from a mixed crust-mantle source or crust source, and the Re content in molybdenite of these deposits is not significantly correlated

Table 12. Pb isotopic characteristics of intrusive rocks and minerals in porphyry molybdenum deposits in the eastern Jilin-Heilongjiang area (after Hou XG, 2017).

Deposit name	Sample no.	Tested sample	$^{206}Pb/^{204}Pb$	$^{207}Pb/^{204}Pb$	$^{208}Pb/^{204}Pb$	Data source
Huojihe	110723-1	Biotite monzogranite	18.734	15.554	38.267	
	110723-5	Biotite monzogranite	19.401	15.606	38.696	
	090817-13	Granitic aplite	19.242	15.589	38.629	
	090817-14	Granitic aplite	19.041	15.592	38.592	
	090817-11	Granitic aplite	19.202	15.612	38.656	
	090817-12	Granitic aplite	19.159	15.596	38.592	
Daheishan	DH-271	Pyrite	18.364	15.576	38.231	Zhou LL et al., 2014
	DH-258	Pyrite	18.336	15.607	38.326	
	DH-259	Pyrite	18.316	15.564	38.186	
	DH-270	Pyrite	18.306	15.586	38.242	
	DH-263	Pyrite	18.297	15.565	38.177	
	DH-305	Pyrite	18.023	15.595	38.309	
	DH-78	Pyrite	18.064	15.583	38.204	
	DH-301	Molybdenite	18.172	15.553	38.106	
	DH-254	Molybdenite	18.293	15.530	38.063	
	DH-255	Molybdenite	18.368	15.540	38.103	
	DH-261	Molybdenite	18.321	15.546	38.124	
	DH-272	Molybdenite	18.427	15.581	38.234	
	DH-192	Qianzuluo granite porphyry	18.697	15.583	38.502	
	DH-193	Qianzuluo granite porphyry	18.708	15.580	38.494	
	DH-194	Qianzuluo granite porphyry	18.705	15.590	38.518	
	DH-195	Qianzuluo granite porphyry	18.657	15.548	38.379	
	DH-96	Qianzuoluo granite diorite	18.731	15.600	38.583	
	DH-97	Qianzuoluo granite diorite	18.671	15.563	38.409	
	DH-292	Qianzuoluo granite diorite	18.711	15.555	38.494	
	DH-293	Qianzuoluo granite diorite	18.720	15.552	38.476	
	DH-296	Changgangling granodiorite	18.488	15.536	38.298	
	DH-297	Changgangling granodiorite	18.437	15.535	38.224	
	Dhs1-1	Granodiorite porphyry	18.590	15.571	38.338	
	Dhs1-2	Granodiorite porphyry	19.196	15.602	38.295	
	Dhs5-1	Granodiorite porphyry	18.458	15.563	38.275	
	Dhs5-2	Granodiorite porphyry	18.473	15.562	38.343	
		Pyrite	18.5454	15.574	38.2499	
		Pyrite	18.346	15.5637	38.2157	
		Pyrite	18.4554	15.5749	38.2634	
Jidetun	JJd1-1	Granodiorite	18.8185	15.5771	38.6824	Zhang Y, 2013
	JJd1-2	Granodiorite	18.7938	15.5769	38.6612	
	JJd2-1	Diorite-porphyrite	19.0123	15.5847	38.3524	
	JJd2-2	Diorite-porphyrite	18.969	15.5862	38.3677	
Fu'anpu	JFa1-1	Adamellite	18.7322	15.5684	38.446	
	JFa1-2	Adamellite	19.1255	15.5878	38.4606	
Xinhualong	Xhl1-1	Diorite-porphyrite	18.8479	15.5967	38.5863	
	Xhl1-2	Diorite-porphyrite	18.7611	15.5903	38.5108	
	Xhl2-1	Granodiorite porphyry	19.2028	15.6144	38.8775	
	Xhl2-2	Granodiorite porphyry	19.2007	15.6131	38.8874	

with their mineralization ages. Different from the molybdenite in the Dexing copper deposit and in the Cordillera and Andes metallogenic belts on the eastern coast of the Pacific Ocean, the molybdenite in the study area has a low Re content, which is similar to the molybdenite formed by partial melting of the thickened lower crust due to crust source transformation or delamination.

Mo isotopes: The $\delta^{98/95}$Mo values of molybdenite in the study area generally fall within the typical Mo isotope range of molybdenite. However, molybdenite of different structures exhibits significantly different Mo fractionation. Specifically, veined molybdenite shows high $\delta^{98/95}$Mo values, while disseminated molybdenite displays low $\delta^{98/95}$Mo values. Regarding the difference in $\delta^{98/95}$Mo values between veined and disseminated molybdenite in molybdenum deposits in the study area, the Daheishan deposit shows the highest difference of 0.79‰, the Luming deposit shows a difference of 0.56‰, and the Fu'anpu and Baoshan deposits show small

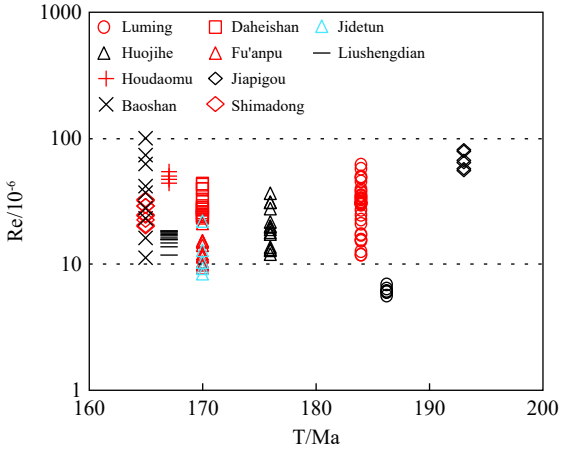

Fig. 12. Re content in molybdenite of typical molybdenum deposits in the eastern Jilin-Heilongjiang area (after Hou XG, 2017).

differences of 0.38‰–0.40‰ (Fig. 13). The large-scale Daheishan and Luming deposits have ore-forming fluids with medium-to-high temperatures and medium-to-high salinities (Fig. 14). In contrast, the small and medium-sized Fu'anpu and Baoshan deposits have ore-forming fluids with medium-to-low temperatures and medium-to-low salinities. Therefore, the temperature and salinity of ore-forming fluids may be the primary factors influencing molybdenite mineralization.

5.3. Tectonic evolution and metallogenic model

Concerning the tectonic framework, the Daheishan deposit lies within the Late Paleozoic−Early Mesozoic Paleo-Pacific tectonic zone and the Meso-Cenozoic circum-Pacific tectonic zone, located to the east of the Xing'an-Mongolian Orogenic Belt. From the Late Permian to the Early Triassic, the Heilongjiang plate, formed by medium and small blocks scattered between the North China and Siberian plates, met the North China plate in the Changchun−Yanji area, commencing the collisional orogeny phase. The Yanshanian marked a geotectonic shift in East Asia (Table 14). Within the study area, this transition period symbolizes the end of the sequential convergence of the Xing'an-Mongolian Orogenic Belt and its neighboring blocks, leading to the formation of the circum-Pacific active continental margin. The Yanshanian tectonic evolution of the Pacific tectonic domain had become the predominant factor constraining the tectonic evolution in the study area. During the Mesozoic, the Izanagi plate moved in the NW13°–NE2° direction, leading to a small angle intersection with Eurasia (Zhu YS et al., 1995). Some scholars suggest that this small-angle oblique subduction is the primary origin of large-scale strike-slip faults, sedimentary basins, and calc-alkaline magmatic belts in eastern China (Zhu X et al., 1983). Therefore, from the Yanshanian Movement or the Jurassic onwards, the tectonic evolution of the circum-Pacific tectonic domain commenced, the study area began to experience Pacific subduction, and the eastern Jilin-Heilongjiang area was part of the circum-Pacific belt (Zhu BQ, 1998). Due to Pacific plate subduction, NNE- and NE-oriented faults were highly developed, controlling regional magmatic activity. Given this specific geotectonic location, the four-stage ore-bearing pluton of the Daheishan deposit is believed to result from hypomagma lodging at the intersections of NNE- and EW-oriented faults. As deep magmas ascended, they crystallized, differentiated, and solidified into rocks continuously. Concurrently, a significant volume of volatile constituents accumulated in the magmas, prompting the cryptoexplosion of molten lava at the magmas' front and leading to the formation of certain-scale cryptoexplosive breccias with low ore-bearing potential. Meanwhile, the intrusion of porphyries formed numerous reticular fissures in the Qiancuoluo granodiorites, which were later filled with ore-forming fluids. During the middle-late mineralization stage, volatile constituents accumulated locally as fissures filled with various veins. As a result, internal pressure increased, leading to local cryptoexplosions and the formation of some small-scale cryptoexplosive breccia pipes (Zhang ZK, 1988). As the sole stock-type molybdenum deposit in northeast China, the Daheishan deposit is unique and distinctive, though it shares similarities with typical porphyry deposits. Its ore-forming parent rocks are calc-alkaline granitic rocks formed in a continental margin compressional tectonic setting. Conversely, the ore-forming parent rocks of the fine-stockwork molybdenum deposits in the western United States (such as the famous Climax molybdenum deposit) are primarily alkaline-calc and alkaline intrusive rocks formed in a continental back-arc extensional tectonic setting. The ore-forming plutons of the Daheishan deposit occur as stocks, differing from the fine-stockwork deposits associated with plutonic intrusions (e.g., the Huojihe and Luming deposits). This study suggests that the Daheishan deposit may be a fine-stockwork stock-type molybdenum deposit occurring in calc-alkaline ore-forming parent rocks.

It is generally believed that a porphyry deposit must be accompanied by deep fault zones nearby, which connect the upper mantle with the upper crust. The Daheishan deposit lies north of the circum-Pacific molybdenum metallogenic belt in eastern China, which evolved as follows: During the Middle and Late Mesozoic, numerous NE- or NEE-trending Mesozoic deep fault zones formed due to the influence of the Pacific tectonic movement; Accompanying these formations was the emplacement and eruption of intermediate-acid magmas. Meanwhile, the intersections of these deep fault zones with the pre-Yanshanian nearly-E-orientated paleo-structures tended to dictate the emplacement sites of intermediate-acid granitoids, thereby forming the Mesozoic tectono-magmatic belt and its associated molybdenum metallogenic belt. The metallogenic evolution of the Jilin-Heilongjiang orogenic belt is as follows: (1) during the Late Triassic, the influence of the circum-Pacific tectonic active zone led to the formation of the NE-trending Dunhua–Mishan translithospheric fault and Yitong–Shulan deep fault and dictated the distribution of regional volcanic-magmatic tectonic belts. Meanwhile, the NE-trending Jilin−Liuhe fault zone, which ran through the mining area, controlled the formation of the volcanic faulted basin in central Jilin; (2) Since

the beginning of the Mesozoic, basement faults, like the Shuanghezhen−Qiancuoluo (Daheishan)−Dadingshan fault zone, displayed extensional characteristics due to the influence of the circum-Pacific tectonic active zone. As a result, an uplift-fault belt with a N-S width of 17 km and a W-E length of nearly 40 km formed, significant in controlling the formation of molybdenum ore fields (Wang CH, 2009); (3) After the Late Triassic, increased fault activity resulted in deep magma upwelling on both sides of several fault-controlled blocks. Intermediate-acid magmas erupted at the

Table 13. Re content in molybdenite of typical molybdenum deposits in the eastern Jilin-Heilongjiang area (after Hou XG, 2017).

Deposit name	Sample no.	Re content/10^{-6}	Data source	Deposit name	Sample no.	Re content/10^{-6}	Data source
Luming	HLM3	12.68	Xu WL et al., 2002	Fu'anpu	FAP-1a	9.94	Li LX et al., 2009
	HLM-4	15.31			FAP-16	11.46	
	HLM-5	15.71			FAP-1c	15.13	
	HLM-5	15.71			FAP-1f	10.52	
	HLM-6	11.90			FAP-1g	11.68	
	06001-1	48.61	Xu WL et al., 2000		FAP-04	15.09	Yao FL et al., 2006
	06001-2	31.58			FAP-07	21.04	
	06001-3	30.40			FAP-08	15.33	
	06401-1	30.87			FAP-09	12.11	
	06401-2	33.54			FAP-12	14.18	
	06401-3	24.60			FAP-23	15.34	
	06401-6	27.09			FAP-29	10.14	
	TWL1-1	33.18			FAP-30	9.38	
	TWL1-2	32.61		Jidetun	JD001	22.04	Yao JJ et al., 2002
	TWL1-3	49.64			JD002	10.39	
	TWL1-4	34.60			JD003	9.32	
	LMD90816-3	57.11	Xu ZG et al., 2008		JD004	12.90	
	LMD90816-1	30.87			JD005	8.42	
	LMD90S16-2	22.66		Dashihe	YB061-1	6.04	Ju N et al., 2012
	LMD90S16-8	30.48			YB061-3	6.94	
	LMD90S16-13	12.01			YB061-4	5.65	
	JDC	17.11			YB061-5	6.09	
	JDC	17.41			YB061-5	6.18	
	LM10	45.24	Yang JH et al., 2003		YB061-6	6.43	
	LM12	48.63		Houdaomu	JHD04-1	50.07	Zhang Y et al,. 2013
	LM17	35.39			JHD04-2	47.12	
	LM11	30.18			JHD04-3	43.82	
	LM14	29.57			JHD04-4	54.23	
	LM13	30.73		Jiapigou	YB010-1	78.43	Zeng PS et al., 2006
	Lm-1	37.28	Yang YC et al., 2010		YB010-2	80.76	
	Lm-2	61.76			YB010-3	63.89	
	Lm-3	30.20			YB010-4	57.06	
	Lm-6	34.73			YB010-5	55.33	
	Lm-15	21.00			YB010-6	66.50	
	Lm-16	39.69		Baoshan	YB064-4	23.09	Zhang D et al., 2017
	Lm-17	38.40			YB064-6	27.83	
Huojihe	TWH1-1	19.80	Zhang H et al., 2007		YB064-8	16.22	
	TWH1-2	21.72			YB064-9	41.61	
	TWH1-4	17.33			YB064-10	36.86	Zhang Y et al., 2013
	TWH1-5	13.19			Jxlun-010	62.30	
	TWH1-3	20.09			Jxlun-014	11.31	
	090817-15	13.69			Jxlun-015	73.24	
	090817-15	12.90			Jxlun-016	99.66	
	090S17-3	12.04		Liushengdian	YB065-1	15.75	Zhao HG et al., 2005
	090817-5	30.92			YB065-2	15.71	
	13HJH11	27.58	Zhang Y et al., 2016		YB065-3	16.80	
	13HJH13	18.91			YB065-4	16.19	
	13HH20	17.92			YB065-5	18.08	
	13HJH22	36.50			YB065-6	17.22	
	13HH25	31.05			JIsm-004	11.88	Zhang Y et al., 2013

Table 13 (*Continued*)

Deposit name	Sample no.	Re content/10^{-6}	Data source	Deposit name	Sample no.	Re content/10^{-6}	Data source
Daheishan	DHS-1a	24.15	Wang CH et al., 2009		JIsm-005	18.43	
	DHS-1d	27.85			JIsm-006	18.34	
	DHS-1e	27.15			JIsm-006	17.67	
	DHS-1h	39.57			JIsm-007	14.81	
	DHS-1i	39.36			JIsm-008	13.76	
	DHS-3a	43.57		Shimadong	B7-1	24.67	Zhu BQ et al., 2001
	DHS-2c	31.03			B7-2	24.24	
	DHS-2e	42.81			B8-1	31.92	
	DHS-3c	29.02			B8-1	32.57	
	DHS-3d	32.68			B10-1	28.91	
	DH-252	27.14	Zhou LL et al., 2014		B10-2	29.06	
	DH-301	24.88			B11-1	22.45	
	DH-255	24.27			B11-2	19.94	
	DH-261	23.95			B11-3	20.46	
	DH-272	28.22					
	DH273	23.38					
	Jdhm-029	25.78	Zhang et al., 2013				

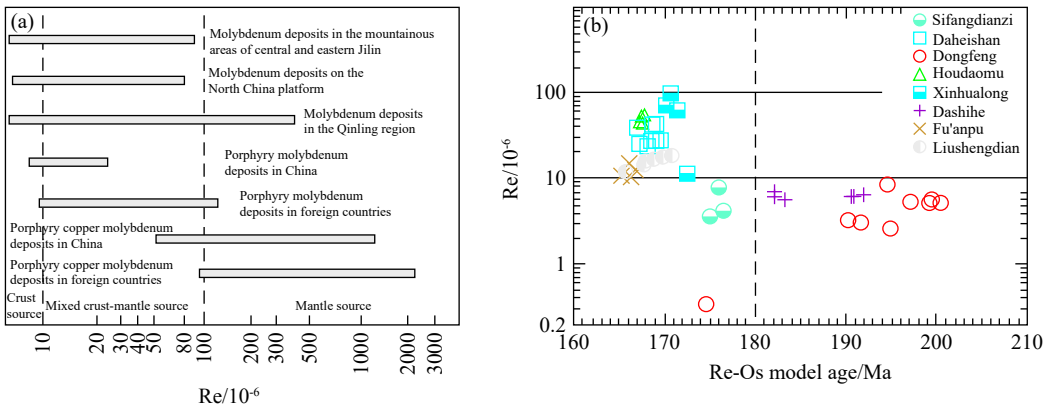

Fig. 13. Comparison of Re content (a) and Re content *vs.* Re-Os model age (b) of molybdenite in typical molybdenum deposits in central and eastern Jilin (after Zhang Y, 2013).

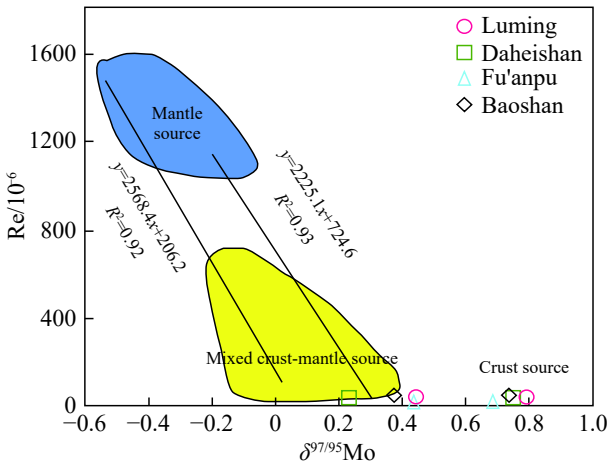

Fig. 14. Re-Mo content pattern of molybdenite in typical molybdenum deposits in the eastern Jilin−Heilongjiang area (after Hou XG, 2017).

junctions of uplifts and faults, followed by the intrusions of mafic magmas and ultramafic-intermediate-acid magmas. Multiple magma intrusions formed the complex plutons of the Daheishan deposit, including Changgangling biotite granodiorites and Qiancuoluo inequigranular biotite granodiorites, granodiorite porphyries, and felsitic granodiorite porphyries in chronological order. The ore bodies in the complex plutons were primarily hosted in the granodiorite porphyry plutons and their surrounding inequigranular granodiorite plutons, and mineralization mainly occurred after magmatism (Wang CH, 2009). The deep magma differentiation during ore body formation increased the molybdenum content in the late plutons, which in turn became increasingly small. During the upward intrusion and solidification of deep magmas, a significant volume of volatile constituents accumulated in the magmas, prompting the cryptoexplosion of molten lava at the magmas' front. As a result, certain-scale cryptoexplosive breccias were formed at the top of the predominant ore-forming granodiorite porphyries. In the late stage of magmatism, hydrothermal fluids rich in potassium, primarily in a high-temperature gaseous state, rose from the deep magma chambers. Along the intergranular pores and structural fractures of rocks, alkaline metasomatism by these fluids resulted in planar biotite-quartz-K-feldspar alteration. Consequently, the quartz content increased gradually, and the quartz filling and metasomatism

Table 14. Geological characteristics of the Daheishan deposit and its adjacent areas (after Ju N, 2020).

Deposit	Fu'anpu	Jidetun	Daheishan	Dashihe	Chang'anpu
Mineral type	Mo	Mo	Mo	Mo	Cu、Mo
Ore-controlling structure	NE- and NW-trending faults	NE- and NW-trending faults	Intersection of NE- and EW-trending faults	NE-trending dominant fault and NW-trending secondary fault	Intersection of NE- and NW- trending faults
Ore-forming plutons and mineralization age	Porphyroid monzogranite	Porphyroid monzogranite, quartz diorite	Granodiorite, granodiorite porphyry	Cryptoexplosive breccia pipe, porphyroid granodiorite	Biotite monzogranite primarily, followed by the cryptoexplosive breccia pipe
Ore body occurrence	Branched/within plutons	Ellipsoidal and stratoid/within plutons	Circular/within plutons	Turbinate /breccia pipe and within plutons	Stratiform, lensoid, veined/quartz veins, within plutons
Surrounding rock alteration	Potassic alteration, sericite alteration, silicification, chloritization, epidote alteration	K-feldspar alteration, sericite alteration, silicification, epidote alteration, kaolinization, greisenization	Silicification, K-feldspar alteration, sericite alteration, propylitic alteration	Sericitization and chloritic alteration	Silicification, potassic alteration, carbonation, chloritic alteration, epidote alteration, argillization, sericite alteration
Ore mineral	Molybdenite, pyrite	Molybdenite, pyrite, chalcopyrite, magnetite, galena, sphalerite	Molybdenite, pyrite, chalcopyrite	Molybdenite, pyrite, chalcopyrite, pyrrhotite, galena, sphalerite	Molybdenite, chalcopyrite, pyrite, magnetite, sphalerite, galena
Data source	Chen YJ et al., 1991; Zhang WH et al., 1993; Zhang Y, 2013				

along fractures led to the formation of K-feldspar or quartz-K-feldspar veins. Disseminated minerals, such as pyrite, molybdenite, chalcopyrite, tetrahedrite, and scheelite, were formed along with the K-silicate alteration in this stage. With a decrease in temperature and mixing of groundwater, ore-bearing fluids converted from a gaseous to a liquid state, and their physical and chemical properties changed accordingly. Further, the oversaturation of silica in the hydrothermal fluids led to the hydrolyzation of a large amount of feldspar, resulting in quartz-sericite alteration and beresite alteration, which were superimposed on the K-silicate alteration zone. As a result of these alterations, a large amount of molybdenite precipitated, and various ore-bearing veins, such as molybdenum-bearing quartz veins, molybdenite veinlets, quartz veins, and carbonate veins, were formed sequentially. After a long period, the mineralization process entered its middle-late stage, when volatile constituents accumulated locally as fissures filled with various veins. As a result, internal pressure increased, leading to local cryptoexplosions and the formation of some small-scale cryptoexplosive breccia pipes. In the late mineralization stage, the temperature dropped further, and groundwater predominated in and diluted the ore-forming fluids to a great extent. This dilution, along with the gradual exhaustion of ore-forming materials, led to carbonation, gypsum alteration, zeolite alteration, and weak pyritization. After this chain of events, the alteration and mineralization process ended, and a typical porphyry molybdenum deposit with concentric alteration and mineralization zoning was formed finally.

In sum, there are two metallogenic models of porphyry molybdenum deposits (Zhang Y, 2013): (1) the mixing and crystallization differentiation between intraplate-type basaltic magmas and overlying magmas from lower-crust melting; (2) the crystallization differentiation of magmas from lower-crust melting coupled with the accumulation and ore-forming processes of ore-bearing fluids. However, a contact metasomatic metallogenic model may also exist in both models. Given the formation of mafic complex-associated copper-nickel sulfide deposits in the study area during the Late Triassic (Local Chronicles Compilation Committee of Yongji County, 1985; Zhang LG., 1989), large-scale basaltic magmas might have existed in the MASH zone at least. During the lengthy cooling of the basaltic magmas, the generated heat might have been crucial for the lower-crust melting and the formation of large-scale granites in the study area. Additionally, some granites with a mixed crust-mantle source formed alongside the intraplating of basaltic magmas. Therefore, this study highlights that the diagenetic and metallogenic model should be as follows (Fig. 15): (1) the underplating of basaltic magmas induced the lower-crust melting, forming magma chambers; (2) ore-bearing fluids formed due to the intraplating of a minor portion of basaltic magmas, the mixing of these basaltic magmas with the magmas from the lower-crust melting, and the fractional crystallization of the magma chambers; (3) these fluids rose and underwent cryptoexplosion after porphyry formation, forming brecciated, veinlet-disseminated, and veined ore bodies successively; (4) these ore bodies made contact with the upper Paleozoic molybdenum-bearing strata, forming a contact metasomatic molybdenum deposit.

5.4. Ore prospecting models

Large-scale mineralization is the product of a certain geodynamic environment (Mao JW et al., 1999; Zhang BT et al., 2003). The study area entered a continental margin environment in which the Pacific plate subducted toward Eurasia during the Early Jurassic. The intense and complex tectono-magmatic processes led to the formation of many molybdenum, gold, and copper deposits in the study area.

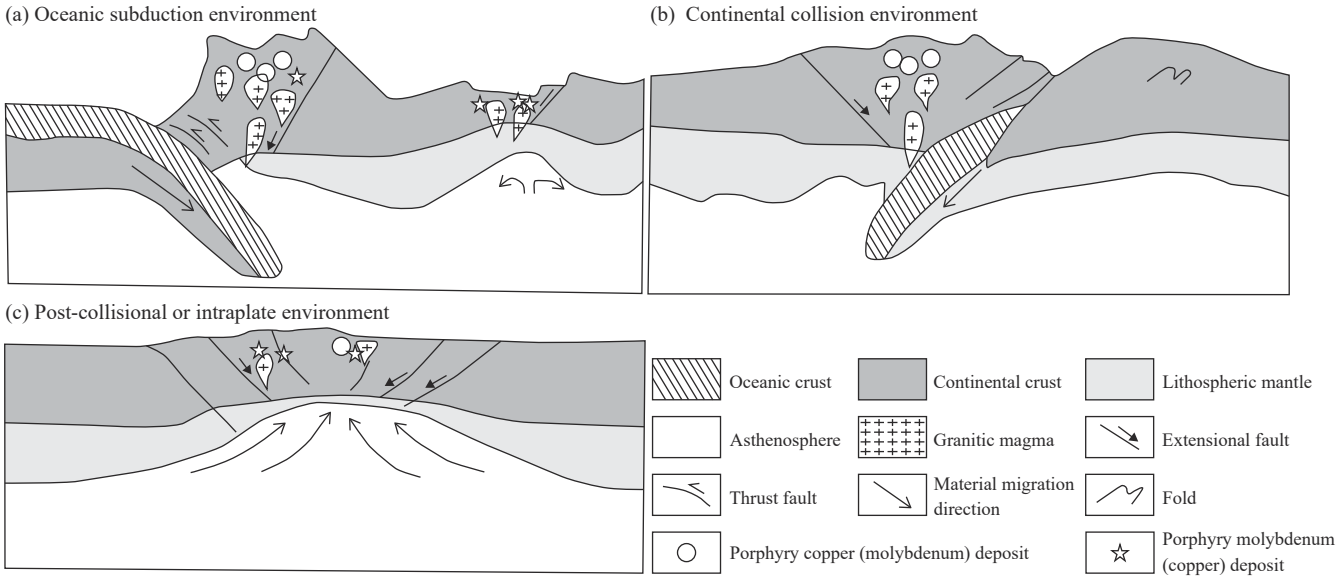

Fig. 15. Schematic of tectonic evolution of typical porphyry molybdenum deposits (after Zhang Y, 2013).

This study thoroughly investigated the metallogenic mechanisms of molybdenum deposits in the study area by analyzing the geological characteristics, ore-forming fluids, geochemistry, and metallogenic chronology of these molybdenum deposits (Fig. 16). Based on the metallogenic models, the metallogenic dynamic model and the integrated gravity-magnetic-magnetotelluric prospecting model have been constructed for endogenetic molybdenum deposits in the study area (Zhang DH et al., 2001; Yuan DS et al., 2012; Zhang Y, 2013).

5.4.1. Metallogenic dynamic model

The geodynamic model of the Daheishan deposit is as follows: During the subduction of the paleo-Pacific plate, fluids metasomatized the basaltic magmas formed by the partial melting of the Proterozoic secondary lithospheric mantle. The basaltic magmas exhibited intraplating and underplating in two mineralization periods. The underplating of the basaltic magmas during the Early Jurassic triggered the lower-crust melting, forming magma chambers, which formed ore-bearing fluids in their late evolutionary stage. Consequently, the Early Jurassic molybdenum deposits, represented by Dongfeng and Jiapigou, formed in eastern Jilin. As the Pacific plate further subducted northwestwards, the continued underplating of basaltic magma caused the lower-crust melting, forming magma chambers. A small portion of basaltic magmas mixed with the magmas from the lower-crust melting, forming ore-bearing fluids in the late evolutionary stage of the magma chambers. Consequently, the Middle Jurassic molybdenum deposits, represented by Daheishan and Fu'anpu, formed in central Jilin (Fig. 17).

5.4.2. Integrated prospecting model

Gravity anomalies: the Bouguer gravity field of the Daheishan deposit area resides within a quasi-circular gravity low area surrounded by the annular Quchaihe-Nanloushan-Wangqi-Yongji-Huangyu-Quchaihe gravity gradient belt. On the 14 km × 14 km moving average residual gravity anomaly map, this gravity low area, which showcases many local gravity lows and highs with different strengths, morphologies, strikes, and scales, is encircled by a continuous bead-like local gravity high zone. Based on the comprehensive analysis of geological data, it can be inferred that the annular Bouguer gravity gradient belt and the annular curve of zero residual gravity anomalies are caused by the annular fault structural zone formed by the intersection of NE-, NW-, EW-, and SN-trending fault belts. The local gravity lows inside are closely related to the intermediate volcanic rocks of the Late Triassic Sihetun Formation, the intermediate and intermediate-acid volcanic rocks of the Early Jurassic Nanloushan Formation, and the Jurassic-Cretaceous intermediate-acid granitoids. The local gravity highs are largely the reflection of the outcropping, semi-outcropping, and concealed Paleozoic basement strata, such as the Early Paleozoic Cambrian Toudaogou Formation, the Late Paleozoic Lower Carboniferous Luquantun Formation, and the Middle Permian Fanjiatun Formation (Table 15). Consequently, it can be inferred that the study area contains well-developed fault structures, which form the hub (center) of tectonic activity in central Jilin. Particularly, the Daheishan annular fault structure, which is jointly formed by the NE-, NW-, EW-, and SN-trending faults, controlled the multi-phase magmatic eruptions and intrusions in the study area. Moreover, this annular fault structure provided rich ore-forming materials for the formation of endogenetic metal minerals, necessary heat sources for mineralization, and favorable space for ore storage. In addition, this annular fault structure controlled the volcanic activity centers at Daheishan and Nanloushan and acted as the fundamental ore-controlling structure of the Daheishan and Nanloushan mineralization concentration areas (ore fields).

Aeromagnetic anomalies: on the 1:50000 aeromagnetic anomaly map, the magnetic field of the ore field hosting the Daheishan deposit is dominated by quasi-circular negative

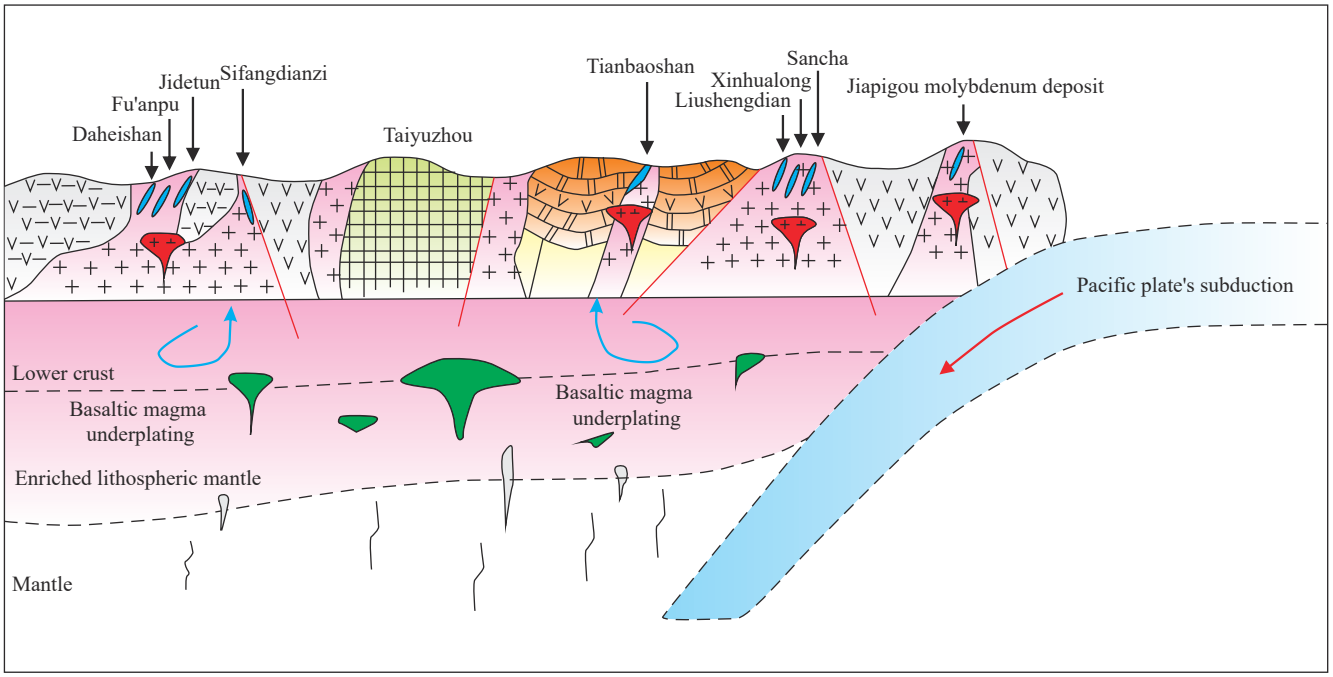

Fig. 16. Metallogenic dynamic model of typical molybdenum deposits in central and eastern Jilin (after Zhang Y, 2013).

anomalies —the Cuoluotun anomalies (area: about 4 km^2; intensity: −100–−200 nT) surrounded by NE-directed annular high magnetic anomalies. The northwestern part of the annular high magnetic anomalies shows a gentle zonal distribution, with the strike shifting from NE to nearly EW from south to north. This part exhibits high continuity of anomaly curves and anomaly intensity of generally 300–500 nT. In contrast, the southeastern part of the annular high magnetic anomalies exhibits a NE-directed arc belt protruding southeastward, a steep northwestern side, a gentle southeastern side, and peaks locally, with intensity mostly exceeding 500 nT and up to maximums of 1500–2000 nT. Furthermore, the northwestern side of this part, which presents significant negative anomalies and low-continuity anomaly curves, can be divided into several small local quasi-circular and elliptical anomalies. The annular high magnetic anomalies are primarily related to the Late Hercynian-Yanshanian magmatic activity in the Daheishan-Toudaogou area. Its northwestern part is induced by Yanshanian intrusive rocks, and its southeastern part is caused by Late Hercynian ultramafic rocks and Yanshanian intermediate-acid intrusive rocks. The Qiancuoluo negative anomalies are related to the ore-bearing complex Changgangling pluton, which, as a plagiogranite pluton, shows negative anomalies due to thermal demagnetization caused by multi-stage magmatic intrusions and hydrothermal alterations. According to the strike of aeromagnetic anomalies, the ore-bearing plutons are primarily controlled by the intersection of NE- and EW-trending faults, which are inferred to be a part of the dominant structural system of the Daheishan ore field.

Integrated gravity-magnetic-magnetotelluric prospecting model: previous researchers conducted multiple surveys around the Daheishan deposit, including 1∶10000 surface magnetic surveys, 1∶25000 spontaneous potential and high-power induced polarization sounding, and gravity surveys along profiles. Ore-bearing plutons responded at varying degrees in these surveys, including high-amplitude anomalies in apparent charging rate (Ms), spontaneous potential (U), and soil molybdenum content and low-amplitude anomalies in gravity and magnetism. Significant application results have been achieved in the Daheishan deposit using the integrated geophysical and geochemical exploration method. As indicators, the obtained three types of high-amplitude anomalies and two types of low-amplitude anomalies provide a comparable, effective model for prospecting similar deposits in the study area.

5.4.3. Prospecting favorable areas

Based on the integrated geological, geophysical, and geochemical prospecting model of the Daheishan deposit, this study performed metallogenic prediction by analyzing the metallogenic geological conditions and the integrated aeromagnetic-gravity-geochemical anomalies in the study area. As a result, three areas with negative aeromagnetic anomalies were selected as favorable sections for the prospecting of molybdenum deposits (Fig. 18).

The negative aeromagnetic anomaly area in northern Miaoling Village: This anomaly area lies about 3.6 km southwest of the Daheishan deposit and about 2.9 km away from the Changgangling molybdenum ore occurrence in the west. This S-N-directed nearly-elliptical anomaly area has a length of 1.5 km, a width of 0.72 km, and edges with high gradients. This area exhibits complete traps, with the lowest anomaly intensity being −36 nT. It is surrounded by four local high-amplitude aeromagnetic anomalies in the north, east, and south and is separated from the western low-gentle positive aeromagnetic anomalies by a distinct anomaly gradient belt in the west. This anomaly area resides at the southern edge of the geochemical overlapping anomalies of molybdenum,

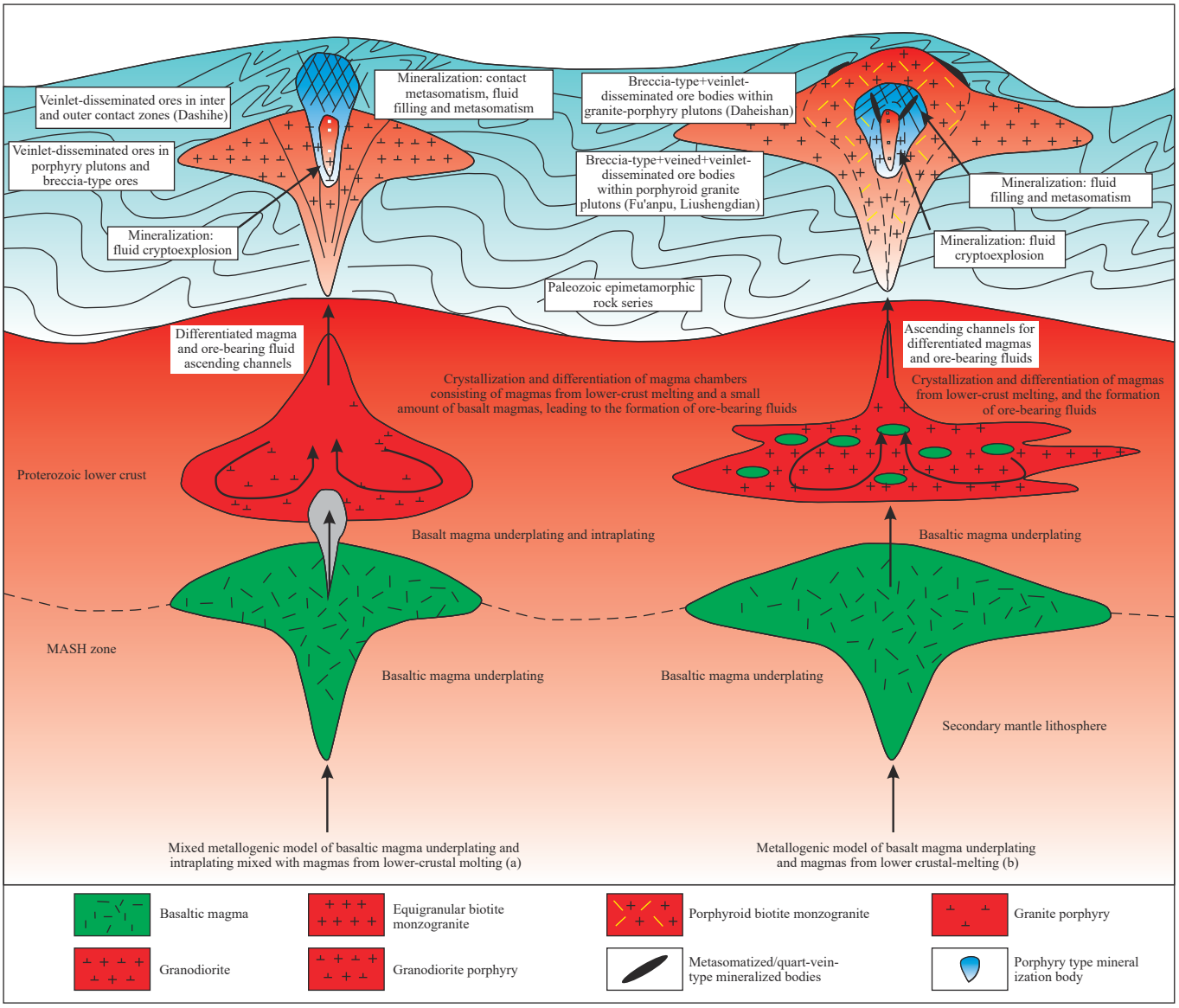

Fig. 17. Metallogenic models of the Daheishan porphyry molybdenum deposit (after Zhang Y, 2013).

tungsten, bismuth, and nickel of the Daheishan deposit.

The negative aeromagnetic anomaly area between Qiancuoluo and Baishi villages: This anomaly area, positioned about 3.2 km northeast of the Daheishan deposit, is an arc-shaped low-amplitude magnetic anomaly area protruding northwestward. It is composed of two splayed negative magnetic anomalies and is embedded in the high-amplitude magnetic anomalies in the southeast. It has a length of 2.6 km, a width of 0.42 km, and a lowest anomaly intensity of −50 nT. This anomaly area lies in the geochemical overlapping anomalies of molybdenum, tungsten, bismuth, and nickel in the Daheishan deposit.

The negative aeromagnetic anomaly area between Xiyang Town and Shuihugou: This anomaly area is lageniform and composed of northern moderate and southern strong negative magnetic anomalies. This anomaly area, with an N-S length of 2.3 km, a W-E width of 0.92 km, and lowest anomaly intensity of −340 nT, is located in the outer zone of the geochemical overlapping anomalies of molybdenum, tungsten, bismuth, and nickel in the Daheishan deposit.

The three negative aeromagnetic anomaly areas are all smaller than the Daheishan deposit. However, they are all situated at the edge of an N-S-directed Yanshanian tectono-magmatic zone, which is also the transition part between the N-S-directed low-amplitude gravity anomaly zone caused by the tectono-magmatic zone and the high-amplitude gravity anomaly zone in the east and southeast. These three anomaly areas share similar metallogenic geological conditions and geophysical and geochemical anomalies with the Daheishan deposit, thus showing high potential for molybdenum prospecting.

6. Conclusions

(i) The ore-controlling structures of the Daheishan deposit are dominated by nearly-EW-trending basement faults and NNE-trending faults. The molybdenum mineralization of the deposit primarily occurred in a veined or veinlet-disseminated

Table 15. Comparison between the Daheishan molybdenum deposit and typical copper molybdenum deposits in the world (after Wang ZG, 2012).

	Calc-alkaline stockwork molybdenum deposit		Alkali-calcic and alkaline stockwork molybdenum deposits			Porphyry copper deposit	
	Stock type	Plutonic intrusion-associated type	Climax type	Alkaline type		Island-arc type	Continental-margin type
				Porphyry	Leucogranite		
Magma series	Calc-alkaline; High-K calc-alkaline		High-K calc-alkaline; alkaline-calcic	Alkaline-calcic; Alkaline		Calcic; calc-alkaline	Calcic; calc-alkaline; alkaline-calcic
$K_{57.5}$ range	1.5–2.5		25–4.4	4.0–6.0		0.4–2.5	0.6 to > 5
Tectonic setting	Convergent continental plate margin		Subduction-associated continental solitary extension ring	Continental solitary extension environment	Continental back-arc discrete environment; cratonic rift zone; rifts associated with oceanic basin stretching; hotspot	Convergent plate margin	Convergent continental plate margin
Paragenetic igneous rock	Quartz monzonite; granite; alaskite; aplite	Granodiorite; quartz monzonite; granite; alaskite	Rhyolite - quartz latite: granite aplite; K_2O > 5%; SiO_2 > 75%	Monzonite-syenite; K_2O+Na_2O > 10%; SiO_2 61%–65%	Leucogranite; K_2O > 5%; SiO_2 73%–76%	Diorite quartz monzonite	Granodiorite- quartz monzonite
Porphyritic texture	Present	Present or not	Present	Present or not	Present	Present or not	Present or not
Chemical composition of rocks							
TiO_2/%	>0.2	0.1–0.2	<<0.2	>0.5	<0.1	>0.3	>0.2
Rb/10^{-6}	150–350	100–350	200–800	No available data	>200	<100	<210
Sr/10^{-6}	300–800	100–800	<125	No available data	<100	500–1000	450–1500
Nb/10^{-6}	<20	<10	25 to > 200	>100	15–140	<5	<20
Hydrothermal system							
Maximum molybdenum reserves/t	300000	1600000	2000000	Small-sized	350000	30000	1500000
MoS_2 content in mineralized zone/%	0.1–0.25	0.1–0.20	0.2–0.49	<0.3	0.25–0.30	<0.01	0.01–0.1
Maximum F content/%	0.1–0.25	0.05–0.15	0.5–2	No available data	1 to > 5	Low	0.04–0.4
Major element	Mo-W-Cu	Mo-Cu-(W)	Mo-F-W-Sn-Zn-Ag-Pb-Cu-U	Mo-F-Sn-W	Mo-F-Sn-W-(Bi)-(As)	Cu-Au-(Mo)	Cu-Mo-Ag-Au-Pb-Zn
HF/HC1 ratio in fluids	Low	Low	High	No available data	No available data	Low	Low
Multiple mineralized crust	None	None	Common	No available data	Yes	No	Rare
Typical deposits	Kitsault; Hall; Buckingham; Daheishan in Jilin	Endako; Adanac; QuartzHill? Mt. Tolman; East Kounrad; Huojihe in Heilongjiang; Luming; Fu'anpu and Jidetun in Jilin	Climax; Urad-Henderson; Mt. Emmons; Pine Grove; Questa*; Mt. Hope*; Glacier Gulch*	Three Rivers stock; Rialto stock	Cave Peak; Malmbjerg; Bordvika; Mt. Pleasant	Panguna; Atlas; Marcopper	Bingham; San Manuel

form within Qiancuoluo granodiorite porphyries and inequigranular granodiorites. The ore types of the deposit encompass the veinlet-disseminated type, the quartz veinlet-stockwork type, and the breccia type. The surrounding rocks' alterations exhibit annular alteration zonation consisting of the beresite, quartz-sericite, and propylite alteration zones outward from the porphyry plutons as the center. The mineralization of the deposit mainly occurred during the hydrothermal mineralization period, which can be divided into the quartz-molybdenite-pyrite stage, the quartz-

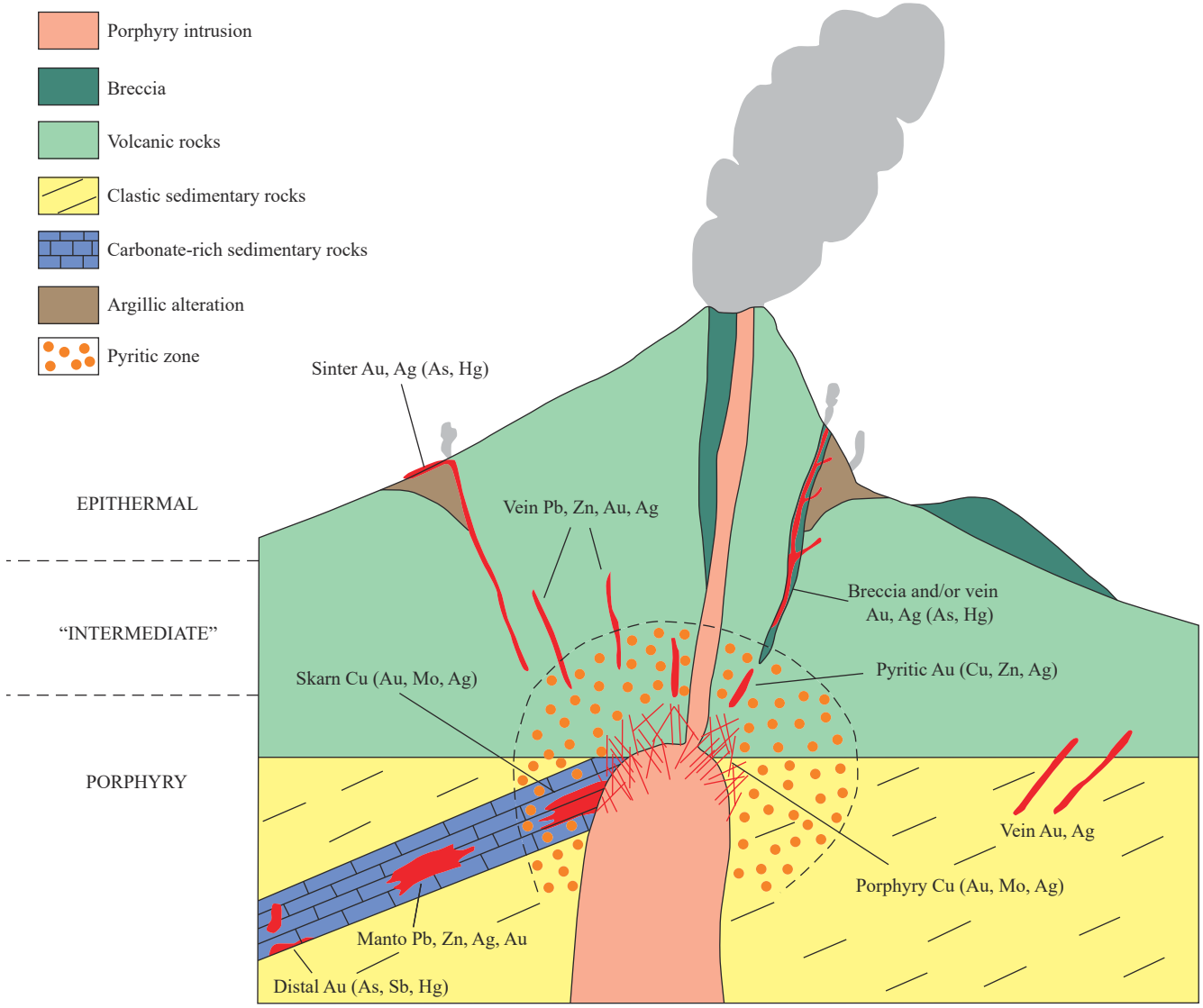

Fig. 18. Prospecting model of the Daheishan molybdenum deposit (after Zhang Y, 2013).

polymetallic-sulfide-molybdenite stage, and the quartz-carbonate-fluorite stage.

(ii) The initial ore-forming fluids of the Daheishan deposit were characterized by a deep sulfur source. The fluid inclusions primarily include daughter mineral-bearing three-phase inclusions and two-phase vapor-liquid inclusions. The ore-forming fluids pertain to an H_2O-NaCl-CO_2 system with low CO_2 content, exhibiting medium-to-high temperatures and medium-to-high salinities. These fluids primarily originated from magmatic water, with fluid boiling contributing largely to mineral precipitation.

(iii) The complex plutons associated with molybdenum mineralization in the Daheishan deposit mainly consist of the Changgangling and Qiancuoluo plutons. The zircon U-Pb ages of Changgangling monzogranites, Qiancuoluo granodiorite porphyry, and Qiancuoluo porphyroid granodiorites are approximately 178 Ma, 169 Ma, and 170 Ma, respectively, indicating an Early Yanshanian diagenetic age. The magma source of the ore-forming plutons associates closely with the mantle, and the formation of ore-forming plutons is related to the partial melting of the thickened juvenile crust under the action of plate subduction. In the early mineralization stage, the partial melting of lower-middle crustal materials at low pressure formed monzogranites with typical island arc magmatic properties. Later, the partial melting of lower crustal materials at relatively high pressure formed adakitic granodiorite porphyries.

(iv) The metallogenic model of the Daheishan deposit is as follows: During the Early-Middle Jurassic, the crust in central and eastern Jilin began to accrete and thicken under the influence of the Pacific plate's subduction. Concurrently, mantle-derived basaltic magmas upwelled and underplated, and the partial melting of lower-middle crustal materials commenced, forming typical island arc magmas at low pressure. The upward intrusion of these magmas led to the formation of large-scale Changgangling granitoids, which form the periphery of the complex plutons of the deposit. With the continuous subduction of the Pacific plate, the asthenosphere continued to upwell, increasing the pressure. After partial melting, the juvenile basaltic lower crustal

materials formed adakitic magmas, which solidified into Qiancuoluo granodiorite porphyries and inequigranular granodiorites. As ore-bearing fluids and volatile constituents escaped from the magmatic-hydrothermal system and intruded upward along structural fractures, they filled and metasomatized the Qiancuoluo granodioritic plutons for enrichment and mineralization, forming the Daheishan deposit. The Qiancuoluo granodiorite porphyries, which are more closely related to mineralization, are the ore-forming plutons. The Changgangling plutons provide a part of the ore-forming materials and serve as favorable ore-forming surrounding rocks.

(v) Based on the integrated geological, geophysical, and geochemical prospecting model of the Daheishan deposit, this study performed metallogenic prediction by analyzing the metallogenic geological conditions and the integrated aeromagnetic-gravity-geochemical anomalies in the study area. As a result, three areas with negative aeromagnetic anomalies were selected as favorable sections for the prospecting of molybdenum deposits. The three negative aeromagnetic anomaly areas are all smaller than the Daheishan deposit. However, they are all situated at the edge of an N-S-directed Yanshanian tectono-magmatic zone, which is also the transition part between the N-S-directed low-amplitude gravity anomaly zone caused by the tectono-magmatic zone and the high-amplitude gravity anomaly zone in the east and southeast. These three anomaly areas share similar metallogenic geological conditions and geophysical and geochemical anomalies with the Daheishan deposit, thus showing high potential for molybdenum prospecting.

CRediT authorship contribution statement

Nan Ju designed the conceptualization, presented the idea, and wrote the manuscript with input from all authors. Di Zhang contributed to the investigation, data curation, and visualization. Guo-bin Zhang carried out the sample preparation and formal analysis. Bao-shan Liu supervised the findings of this work. All authors discussed the results and contributed to the final manuscript.

Declaration of competing interest

The authors declare no conflicts of interest.

Acknowledgement

The authors would like to extend their gratitude to Researcher De-ming Sha, who reviewed this paper and made valuable comments, and to Researcher Zhi-guo Hao, who recommended preparing this paper and offered valuable opinions. This study was jointly funded by a project of the National Natural Science Foundation of China (42102087), a project of the China Postdoctoral Science Foundation (2022M712966), and a key special project of the Ministry of Science and Technology of China (2021QZKK0304).

References

Bi SY, Wang DR, Jia DC, Shao JB. 1995. The basic characteristics of the structure of the terrain in Jilin Province. Jilin Geology, 14(1), 1–14 (in Chinese with English abstract).

Cai JH, Yan GH, Xiao CD, Wang GY, Mu BL, Zhang RH. 2004. Nd, Sr, Ph isotopic characteristics of the Mesozuicintrusive rocks in the Taihang-Da Hinggan Mountains Tectonomagmatic Bclt and thcir source region. Acta Petrologica Sinica, 20(5), 1225–1242 (in Chinese with English abstract).

Chang C, Sun JG. 2007. Study on metallogenic regularity and minerallizition conditions of the porphyry type polymetallic ore deposit in eastern Jilin province: Taken Xiaoxinancha gold-copper deposit as an example. Journal of Changchun Institute of Technology (Natural Science Edition), 16(25), 56–60 (in Chinese with English abstract).

Chen JS, Ge WC, Chen HJ, Xing DH, Liu M, Li WW. 2015. Geochemistry and genesis of the host rock of Daheishan molybdenum deposit in Yongji, Jilin Province. Geology and Resources, 24(2), 93–101 (in Chinese with English abstract). doi: 10.13686/j.cnki.dzyzy.2015.02.003.

Chen WM. 1984. Mineral sources and evaluation marks of porphyry copper deposits in China. Journal of Institute of Mineral Deposits, Ministry of Geology and Mineral Resources, 1984(2), 1–78 (in Chinese with English abstract).

Chen WM. 2002. On genesis of porphyry copper deposit. Geoscience, 16(1), 1–8 (in Chinese with English abstract).

Chen YJ, Ni P, Fan HR, Pirajno F, Lai Y, Su WC, Zhang H. 2007. Diagnostic fluid inclusions of different types hydrothermal gold deposits. Acta Petrologica Sinica, 23(9), 2085–2108 (in Chinese with English abstract).

Chen YC. 1991. Prospective evaluation of mineral resources in main metallogenic belt of China, Beijing, Geological Publishing House, 16–46 (in Chinese with English abstract).

Chen YC, Zhu YS. 1993. Metallogenic models of ore deposits in China. Beijing, Geological Publishing House, 17–23 (in Chinese with English abstract).

Deng PL, Yang XD, Huang Q and Chen YX. 1987. Geophysical field characteristics of Daheishan porphyry molybdenum deposit. Jilin Geology, 24(2), 20–33 (in Chinese with English abstract).

Dong SB. 1986. Metamorphism in China and its relation to crustal evolution. Beijing, Geological Publishing House, 1–235 (in Chinese with English abstract).

Du AD, Zhao DM, Wang SX, Sun DZ, Liu DY. 2001. Precise Re-Os Dating for Molybdenite by ID-NTIMS with Carius Tube Sample Preparation. Rock and Mineral Analysis, 20(4), 247–252 (in Chinese with English abstract).

Gao HM. 1995. Review of research on porphyry copper deposits. Advances in Earth Science, 10(1), 40–46 (in Chinese with English abstract).

Ge WC, Wu FY, Zhou CY, Zhang JH. 2007. Metallogenic age and geodynamic significance of porphyry Cu and Mo deposits in eastern Xing-Mongolia orogenic Belt. Chinese Science Bulletin, 52(20), 2407–2416 (in Chinese with English abstract). doi: 10.1360/csb2007-52-20-2407.

Ge WC, Wu FY, Zhou CY, Rahman A. 2005. The age of the Tahe granitic body in the northern Greater Khingan Mountains and its restriction on the tectonic attribution of the Erguna Block. Chinese Science Bulletin, 50(12), 1239–1247 (in Chinese with English abstract). doi: 10.1360/csb2005-50-12-1239.

Ge XH. 1990. Geotectonic environment and evolutionary profile of eastern Jilin Province. Geoscience, 4(1), 107–1131 (in Chinese with English abstract).

Han CM, Xiao WJ, Windley BF, Zhao GC, Su BX, Ao SJ, Zhang JE,

Zhang ZY, Wan B, Cui B, Qu WJ, Du AD. 2014. Re-Os Age of Molybdenite from the Daheishan Mo Deposit in the Eastern Central Asian Orogenic Belt, NE China. Resource Geology, 64(4), 379–386. doi: 10.1111/rge.12047.

Han YW, Ma ZD. 2003. Geochemistry. Beijing, Geological Publishing (in Chinese with English abstract).

Hou ZQ, QuXM, Wang SX, Gao YF, Du AD, Huang W. 2003. Re-os age of molybdenite deposits in Gangdite porphyry copper belt, Tibet Plateau: Metallogenic duration and application of kinetic background. Science in China(Series D), 33(7), 609–6181 (in Chinese with English abstract).

Hou XG. 2017. Mesozoic metallogenetic granitoids from porphyry Mo deposit in the eastern Jilin-Heilongjiang provinces: Petrogenesis and Molybdenum mineralization. Changchun, Jilin University, Ph. D thesis, 6–155 (in Chinese with English abstract).

Hu SX. 1988. Geology and mineralization of North and South China paleo-plate convergence belt. Nanjing, Nanjing University (in Chinese with English abstract).

Ji KJ, Wu XH, Zhang GB. 2011. Mineral source, water source, hydrothermal and mineral deposit distribution law. Beijing, Beijing Science and Technology (in Chinese with English abstract).

Jiang PM. 1989. Fundamentals of geothermodynamics. Beijing, Science (in Chinese with English abstract).

Ju N, Ren YS, Wang C, Wang H, Zhao HL, Qu WJ. 2012. Ore genesis and molybdenite Re-Os dating of Dashihe molybdenum deposit in Dunhua, Jilin. World Geology, 31(01), 68–76 (in Chinese with English abstract). doi: 10.3969/j.issn.1004-5589.2012.01.008.

Ju N. 2020. Metallogenic regularity and prospective prediction of porphyry molybdenum deposits in central Jilin Province, NE China. Changchun, Jilin University, Ph. D thesis, 1–117 (in Chinese with English abstract).

Li CY, Tang YQ. 1983. Paleoasian Plate Division and Related Problems. Acta Geologica Sinica, 57(1), 1–9 (in Chinese with English abstract).

Li JA, Cai HY, Wang JY. 1984. Porphyry Copper Mine in China. Beijing, Science Press, 1–150 (in Chinese with English abstract).

Li JH, Xia DX. 1978. Handbook of Isotopic Age Calculation. Beijing, Atomic Energy (in Chinese with English abstract).

Li LX, Song WY, Wang DH, Wang CH, Qu WJ, Wang ZG, Bi SY, Yu C. 2009. Re-Os Isotopic Dating of Molybdenite from the Fu′anpu Molybdenum Deposit of Jilin Province and Discussion on Its Metallogenesis. Rock and Mineral Analysis, 28(3), 283–287 (in Chinese with English abstract).

Li N. 1993. High Temperature Gas Magmatic Diagenesis and Geoliquid Mineralization. Journal of Institute of Mineral Deposits, Chinese Academy of Geological Sciences, (1), 28–51 (in Chinese with English abstract).

Li T. 1963. Average Chemical Composition of Magmatic Rocks in China. Acta Geologica Sinica, 43(3), 271–280 (in Chinese with English abstract).

Liu B. 2001. Density and Isochoric Formulae for NaCl-H2O Inclusions with Medium and High Salinity and Their Applications. Geological Review, 47(6), 617–622 (in Chinese with English abstract).

Liu B, Guan GX. 1987. Density Formulas and Isovolumetric Formulas of Na Cl-H2O Solution Inclusions and Their Applications. Acta Mineralogica Sinica, 7(4), 345–352 (in Chinese with English abstract).

Liu B, Shen K. 1999. Fluid Inclusion Thermomechanics. Beijing, Geological Publishing House, 1–2900 (in Chinese with English abstract).

Lu HZ. 1990. Geochemistry of Inclusions. Beijing, Geological Publishing House, 1–242 (in Chinese with English abstract).

Lu HZ, Chi GX, Wang ZG. 1995. Genesis and Tectonic Environment of Typical Metal Deposits. Beijing, Geological Publishing (in Chinese with English abstract).

Lu HZ, Fan HR, Ni P, Ou GX, Shen K, Zhang WH. 2004. Fluid Inclusion. Beijing, Science Press, 1–444 (in Chinese with English abstract).

Lu JM, Chen GP, Ding W. 2007. Construction of 3D ore body model of Daheishan Molybdenum Mine. Mining Engineering, 5(3), 68–70 (in Chinese with English abstract).

Lu ZQ. 2017. Geology, Geochemistry and Genesis of Daheishan Molybdenum Deposit in the Central Jilin Province. Changchun, Jilin University, Ph. D thesis, 5–75 (in Chinese with English abstract).

Luo MJ, Zhang FM, Dong QY. 1991. Molybdenum deposit in China. Henan Province, Henan Science and Technology Press, 536–538 (in Chinese with English abstract).

Ma HW. 1990. Granitoids and mineralization in Yulong porphyry copper belt, Xizang Province. Wuhan, China University of Geosciences Press (in Chinese with English abstract).

Mao JW, Zhang ZC, Zhang ZH, Du AD. 1999. Re-Os isotopic dating of molybdenites in the Xiaoliugou W (Mo) deposit in the northern Qilian mountains and its geological significance. Geochimica et Cosmochimica Acta, 63(11–12), 1815–1818. doi: 10.1111/1755-6724.12378-42.

Pei RF. 1995. Mineral deposit model in China. Beijing, Geological Publishing House, 39–42 (in Chinese with English abstract).

Qu XM, Hou ZQ and Li YG. 2004. Melt components derived from a subducted slab in late orogenic ore-bearing porphyries in the Gangdese copper belt, southern Tibetan plateau. Lithos, 74(3–4), 131–148.

Rui ZY, Huang CK, Qi GM, Xu J, Zhang MT. 1984. Porphyry Copper (Molybdenum) Deposits in China. Beijing, Geological Publishing House, 1–350 (in Chinese with English abstract).

Rui ZY, Zhang LS, Chen ZY, Wang LS, Liu YL, Wang YT. 2004. Discussion on source rock or source area of porphyry copper deposit. Acta petrologica Sinica, 20(2), 229–238 (in Chinese with English abstract). doi: CNKI:SUN:YSXB.0.2004–02–004.

Shan WL, Zong HL. 1991. Theoretical method and practice of structural deformation analysis. Beijing, China University of Geosciences Press (in Chinese with English abstract).

Shao JL. 1990. Mineralogy of gold prospecting. Beijing, China University of Geosciences Press, 1–158 (in Chinese with English abstract).

Shi ZY, Zhou ZH, Wang YZ, Meng GC, Yang ZG, Yu HW, Li C. 2008. Application effect of prospecting geochemical method in discovery process of large and medium-sized molybdenum deposits in central Jilin Province. Jilin Geology, 27(2), 90–96 (in Chinese with English abstract).

Sun FY, Jin W, Li BL. 2000. Consideration on metallogenic depth of vein hydrothermal gold deposit. Journal of Changchun University of Science and Technology, 30, 27–30 (in Chinese with English abstract).

Sun SS, McDonough WF. 1989. Chemical and isotopic systematics of oceanic basalts: implications for mantle composition and processes. London, Geological Society Special Publications, 313–345.

Sun WD, Zhang H, Ling MX, Ding X, Chung SL, Zhou JB, Yang XY, Fan WM. 2011. The genetic association of adakites and Cu-Au ore deposits. International Geology Review, 53(5–6), 691–703. doi:10.1080/00206814.2010.507362.

Tang KD, Ju N, Zhang DQ, Zhang GB, Feng Y, Kong JG. 2022. Implication of the tectonic evolution of paleo-asian ocean. Geology and Resources, 31(3), 246–258, 330 (in Chinese with English abstract).

Tang RL, Luo HS. 1995. Geology of Yulong porphyry copper (molybdenum) ore belt in Xizang Province. Beijing, Geological Publishing House (in Chinese with English abstract).

Tu GZ. 1988. Geochemistry of stratified deposits in China. Beijing, Science Press (in Chinese with English abstract).

Wang CH, Song YY, Wang DH, Li LX, Yu C, Wang ZG, Qu WJ, Du AD, Ying LJ. 2009. Rhenium-osmium isotopic dating of molybdenite and its geological significance in Daheishan superlarge molybdenum deposit, Jilin Province. Rock and Mineral Analysis, 28(3), 269–273 (in Chinese with English abstract).

Wang L. 2012. Study on the Geological Features and Metallogenic Model of Daheishan Molybdenum Deposit, Jilin Province. Changchun, Jilin University, Ph. D thesis, 6–75 (in Chinese with English abstract).

Wang Q, McDermott F, Xu JF, Bellon H, Zhu YT. 2005. Cenozoic K-rich adakitic volcanic rocks in the Hohxil area, northern Tibet: lower-crustal melting in an intracontinental setting. Geology, 33(6), 465–468. doi: 10.1130/G21522.1.

Wang Q, Wyman DA, Xu JF, Jian P, Zhao ZH, Li CF, Xu W, Ma JL, He B. 2007. Early Cretaceous adakitic granites in the Northern Dabie Complex, central China: Implications for partial melting and delamination of thickened lower crust. Geochimica Et Cosmochimica Acta, 71(10), 2609–2636. doi: 10.1016/j.gca.2007.03.008.

Wang YD, Zhai YY, Lu ZL. 1986. Geological research report of Daheishan Molybdenum Deposit in Yongji County, Jilin Province.1–234 (in Chinese with English abstract).

Wang ZG, Niu JH, Zhu WF. 2011. Ore-forming fluid characteristics and metallogenic mechanism of Antuhaigou gold deposit in Jilin Province. World Geology, 30(3), 313–322 (in Chinese with English abstract).

Wang ZG. 2012. Study on metallogenesis of Mesozoic endogenetic metal deposits in the eastern part of Jilin province. Changchun, Jilin University, Ph. D thesis, 5–175 (in Chinese with English abstract).

Wei JY, Wang GY. 1987. Isotope Geochemistry. Beijing, Geological Publishing House (in Chinese with English abstract).

Wu G, Sun FY, Zhao CS, Li ZT, Zhao AL, Pang QB, Li GY. 2005. Discovery of post-Early Paleozoic collisional granites in the northern margin of the Erguna Block and its geological significance. Chinese Science Bulletin, 50(20), 2278–2288 (in Chinese with English abstract). doi: 10.1360/972004-679.

Wu FY, Jahn BM, Wilde S, Sun DY. 2000. Phanerozoic crustal growth: U-Pb and Sr-Nd isotopic evidence from the granites in northeastern China. Tectonophysics, 328(1–2), 89–113. doi: 10.1016/S0040-1951(00)00179-7.

Wu FY, Sun DY, Ge WC, Zhang YB, Grant ML, Wilde SA, Jahn BM. 2011. Geochronology of the Phanerozoic granitoids in northeastern China. Journal of Asian Earth Sciences, 41(1), 1–30. doi: 10.1016/j.jseaes.2010.11.014.

Wu FY, Yang JH, Lo CH, Wilde SA, Sun DY, Jahn BM. 2007. The Heilongjiang Group: A Jurassic accretionary complex in the Jiamusi Massif at the western Pacific margin of northeastern China. Island Arc, 16(1), 156–172. doi: 10.1111/j.1440-1738.2007.00564.

Woodcock JR, Hollister VF. 1978. Porphyry molybdenite deposits of the North American cordillera. MinePals. Sai. Engng, 10, 3–18.

Xia B, Tu GC, Chen GW, Yu XX. 2000. Global geological setting for the formation of super large porphyry copper deposits. Bulletin of Mineralogy, Petrology and Geochemistry, 19(4), 406–408 (in Chinese with English abstract). doi: CNKI:SUN:KYDH.0.2000-04-073.

Xiao QH, Deng JF, Ma DQ. 2002. Thinking and methods of granite research. Beijing, Geological Publishing House, 1–294 (in Chinese with English abstract).

Xing SW, Zhang HX, Li LY. 2005. Metallogenic geological setting and metallogenic system division of nonferrous metals and noble metals in continental margin of Northeast China. Geology and Resources, 14(3), 181–186 (in Chinese with English abstract).

Xing K. 2021. Constraints on the formation of the Jurassic porphyry Mo mineralization in the Lesser Xing 'an-Zhangguangcai Range, Northeastern China. Beijing, China University of Geosciences (Beijing), Ph. D thesis, 6–67 (in Chinese with English abstract).

Xu JF, Shinjo R, Defant MJ, Wang Q, Rapp RP. 2002. Origin of Mesozoic adakitic intrusive rocks in the Ningzhen area of east China: Partial melting of delaminated lower continental crust? Geology, 30(12), 1111–1114. doi: 10.1130/0091–7613(2002)030<1111:OOMAIR>2.0.CO;2.

Xu ZW, Lu XC, Yang RY, Xie XJ, Ren QJ. 2000. Geological and geochemical characteristics and genesis of Shangfang porphyry molybdenum deposit in Luanchuan County, Henan Province. Geology and Exploration, 36(1), 14–16 (in Chinese with English abstract).

Xu ZG, Chen YC, Wang DH, Lin WW. 2008. Scheme of metallogenic belt division in China. Beijing, Geological Publishing House, 71–74 (in Chinese with English abstract).

Yang JH, Wu FY, Wilde SA. 2003. A review of the geodynamic setting of large-scale Late Mesozoic gold mineralization in the North China Craton: an association with lithospheric thinning. Ore Geology Reviews, 23(3–4), 125–152. doi: 10.1016/S0169-1368(03)00033-7.

Yang YC, Guo J, Zhang LL, Wang KY. 2010. Study on fluid inclusions in Moshishan copper-polymetallic deposit of Heilongjiang. World Geology, 29(2), 313–322 (in Chinese with English abstract).

Yao FL, Sun FY. 2006. Mineral Deposits Course. Beijing, Geological Publishing House, 1–254 (in Chinese with English abstract).

Yao JJ, Zhang SL, Cao LH. 2002. Comprehensive information prospecting model for major large nonferrous and precious metal deposits in China. Beijing, Geological Publishing House, 6–11 (in Chinese with English abstract).

Local Chronicles Compilation Committee of Yongji County. 1985. Annals of Yongji County. Changchun, Jilin Publishing House (in Chinese with English abstract).

Yu XQ, Chen W, Li W. 2008. Geological characteristics and prospecting significance of Dasuji porphyry molybdenum deposit in Inner Mongolia. Geology and Exploration, 44(2), 29–37 (in Chinese with English abstract).

Yuan DS, Xu XB, Wang DD, Li N. 2012. Geophysics features and prospecting direction of Yongji Daheishan porphyry molybdenum deposit. Jilin Geology, 31(4), 60–61 (in Chinese with English abstract).

Zeng PS, Hou ZQ, Gao YF, Du AD. 2006. Re-Os age and mineralization of the Himalayan Cu-Mo - gold deposit in the eastern part of the Indo-Asian Collision Belt. Geological Review, 52(1), 72–84 (in Chinese with English abstract).

Zhang BT, Ling HF, Chen PR. 2003. Problems and solutions in the geochemical correlation of trace elements in multiple systems. Earth and Environment, 31(4), 102–106 (in Chinese with English abstract).

Zhang D, Ju N, Zhang S, Kou LL, Gu YC. 2017. Geochemical characteristics and geological implication of the ore-forming rocks of the changanpu Mo (-Cu) deposit in jilin province. Geology and Resources, 26(3), 253–259 (in Chinese with English abstract).

Zhang DH, Zhang WH, Xu GJ. 2001. Study on Metallogenic Characteristics of Porphyry Metallogenic System. Earth Science Frontiers, 8(3), 193–202 (in Chinese with English abstract).

Zhang H, Li ZW, Zhao C, Cui YR, Xiao YC, Li W. 2007. Regional geology of molybdenum mineralization in Jilin Trough area-Overview of geochemical characteristics. Jilin Geology, 26(2), 51–55 (in Chinese with English abstract).

Zhang LG. 1989. Theory of diagenesis and mineralization and prospecting–Stable isotope geology of major types of deposits and granites in China. Beijing, Beijing University of Technology Press, 84–94 (in Chinese with English abstract).

Zhang WH, Chen ZY. 1993. Fluid Inclusion Geology. Hubei, China University of Geosciences Press, 1–240 (in Chinese with English abstract).

Zhang YB, Wu FY, Wilde SA, Zhai MG, Lu XP, Sun DY. 2004. Zircon

U-Pb ages and tectonic implications of 'Early paleozoic' granitoids at Yanbian, Jilin Province, northeast china. Island Arc, 13(4), 484–505. doi: 10.1111/j.1440–1738.2004.00442.x.

Zhang Y, Sun JG, Xing SW, Zhao KQ, Ma YB, Zhang ZJ, Wang Y. 2016. Ore-forming granites from Jurassic porphyry Mo deposits, east-central Jilin Province, China: geochemistry, geochronology, and petrogenesis. International Geology Review, 58(9), 1158–1174. doi: 10.1080/00206814.2016.1150213.

Zhang Y, Xing SW, Song QH, Wang Y, Yu ZT, Du XH, Ma YB, Zhang ZJ. 2015. Re-Os and U-Pb Geochronology of Porphyry and Skarn Types Copper Deposits in Jilin Province, NE China. Resource Geology, 65(4), 394–404. doi: 10.1111/rge.12074.

Zhang Y. 2013. Research on Characteristics of Geology, Geochemistry and Metallogenic Mechanism of the Jurassic Molybdenum Deposits in the Mid-East Area of Jilin. Changchun, Jilin University, Ph. D thesis, 5–103 (in Chinese with English abstract).

Zhang ZK. 1988. Types and typical geological characteristics of nonferrous metal deposits in Jilin Province. Jilin Geology, 02, 102–114 (in Chinese with English abstract).

Zhao HG, Yao FL, Sun JG. 2005. Study on Metallogenic regularity and Metallogenic conditions of porphyry polymetallic deposit in Eastern Jilin Province–A case study of Xiaoxanancha Au-copper Deposit. Gold, 7(26), 12–14 (in Chinese with English abstract).

Zhou LL, Zeng QD, Liu JM, Zhang ZL, Duan XX, Chen WW, Li YC, Wei JJ. 2010. Metallogenic stage and distribution of ore-bearing fissure in Daheishan porphyry molybdenum deposit, Jilin Province. Geology and exploration, 46(3), 448–454 (in Chinese with English abstract).

Zhou LL, Zeng QD, Liu JM, Friis H, Zhang ZL, Duan XX, Lan TG. 2014. Geochronology of magmatism and mineralization of the Daheishan giant porphyry molybdenum deposit, Jilin Province, Northeast China: constraints on ore genesis and implications for geodynamic setting. International Geology Review, 56(8), 929–953. doi: 10.1080/00206814.2014.900728.

Zhu BQ. 1998. Theory and application of isotope system in earth sciences and crust mantle evolution in mainland China. Beijing, Science Press, 1–330 (in Chinese with English abstract).

Zhu BQ, Zhang JL, Tu XL, Chang XY, Fan CY, Liu Y, Liu JY. 2001. Pb, Sr, and Nd isotopic features in organic matter from China and their implications for petroleum generation and migration. Geochimica Et Cosmochimica Acta, 65(15), 2555–2570. doi: 10.1016/S0016–7037(01)00608–1.

Zhu X, Huang CK, Rui ZY. 1983. Porphyry Copper Deposit in Dexing. Beijing, Geological Publishing House, 1–245 (in Chinese with English abstract).

Zhu YS, Mei YX. 1995. Several problems in the study of metallogenic model. Acta Geoscientica Sinica, 2, 182–189 (in Chinese with English abstract).